Quaternary Science Reviews 355 (2025) 109181

Contents lists available at ScienceDirect

Quaternary Science Reviews

journal homepage: www.elsevier.com/locate/quascirev

Peak glacial-to-Heinrich-1 changes in Denmark Strait Overflow and seawater stratification in the Nordic Seas, a switchboard of changes in Atlantic Meridional Overturning Circulation and the 'Nordic Heat Pump'

Michael Sarnthein [a,*], Patrick Blaser [b]

[a] *Institut für Geowissenschaften, University of Kiel, D-24118, Kiel, Germany*
[b] *Institute of Earth Sciences, University of Lausanne, CH-1015, Lausanne, Switzerland*

A R T I C L E   I N F O

Handling editor: I Hendy

Keywords:
Nordic seas
Deep-water formation
Denmark Strait Overflow
Atlantic Meridional Overturning Circulation
Age control of Heinrich stadial 1
Nordic Heat Pump

A B S T R A C T

Today, the sub-surface Denmark Strait Overflow (DSO) and the Iceland-Scotland Overflow form the starting points of the Atlantic Meridional Overturning Circulation and compensate for the poleward flowing Norwegian and Irminger branches of the North Atlantic surface current that drive the 'Nordic Heat Pump'. During peak glacial and early deglacial times, ice sheets on Iceland and Greenland, and ice-induced isostatic and eustatic sea-level changes reduced the Denmark Strait aperture and DSO. Yet, extremely high benthic stable carbon and oxygen isotope values together with very high ventilation ages of bottom waters suggest a north-south density gradient of intermediate-waters and persistent flow of partially Arctic-sourced waters through both Denmark Strait and Faeroe Channel, analogous to today. The arrival of deglacial meltwaters off northern Iceland induced the onset of Heinrich-Stadial 1 near 18.400 yr BP, as derived from ^{14}C-plateau tuning. They caused a tipping point in DSO circulation shown by 3 °C warming, reduced ventilation and ventilation ages of bottom water, moreover, by increased radiogenic Nd isotope signatures at luff-side Site PS2644. These records suggest a sudden subsurface incursion of Atlantic intermediate waters across basaltic sediments from S.E. of Iceland. Deep-water convection off Norway then was replaced by weak brine water formation, coeval with a breakdown of the 'Nordic Heat Pump' evidenced by a temperature drop on Greenland. After 16.2 cal ka, a major meltwater outbreak from the Barents ice shelf led to modified Heinrich-1-style circulation until ~15.1 cal. ka. Conversely, the DSO intensified during interstadial and Holocene times, causing sediment hiatuses at Site PS2644.

Plain language summary

Differences in salt content of North Atlantic surface waters control variations in Nordic Seas' overturning circulation. These form a switchboard for changes in the oceanic heat transport to North European high latitudes, the 'Nordic Heat Pump', and for the Atlantic Meridional Overturning Circulation (AMOC). We deduced changes in the Nordic Seas' overturning circulation during the peak last glacial and early deglacial (22-15 cal. ka) from two high-resolution marine sediment cores with centennial-scale age resolution based on the technique of radiocarbon plateau tuning. Sediment data suggest that the salinity of surface water, advected from the North Atlantic, started to drop about 18,400 years ago. This drop accompanied a 3 °C rise in temperature and reduced ventilation and radiocarbon ventilation ages of Denmark Strait Overflow waters feeding the AMOC. Off Norway it paralleled a massive rise in the radiocarbon reservoir age of surface waters up to 2000 yr and an abrupt breakdown of Nordic Seas' deep-water convection. Accordingly, Atlantic waters were replaced by less saline polar waters, marking a breakdown of the 'Nordic Heat Pump' and start of 'Heinrich Stadial 1′ as reflected by a coeval cooling documented on top of the Greenland ice sheet, lasting until ~15.1 cal. ka.

* Corresponding author.
E-mail address: michael.sarnthein@ifg.uni-kiel.de (M. Sarnthein).

https://doi.org/10.1016/j.quascirev.2025.109181
Received 9 May 2024; Received in revised form 24 November 2024; Accepted 1 January 2025
Available online 3 March 2025

1. Introduction

The Denmark Strait Overflow (DSO; Fig. 1) with its exceptionally high density plays a key role for the lower branch of the Atlantic meridional overturning circulation (AMOC) and thereby, for global deep-ocean circulation. The DSO is closely associated with the "Nordic Heat Pump", that is the poleward advection of warm Atlantic waters off Norway. Therefore, any DSO changes have major implications for northern hemispheric climate (Jansen et al., 2020), moreover, they are crucial for deep-ocean ventilation and (radio)carbon uptake (Sarnthein et al., 2015). Today, the flux of DSO is long-term fairly stable with >3 Sv entering from the southern Greenland Sea and Arctic Ocean (Brakstad et al., 2023). Further 5 Sv are entrained into DSO during its overflow in the Irminger Sea to the south of the Denmark Strait, where a 2.5 km deep descend acts in stabilizing the DSO (data of Biastoch et al., 2003, 2021; Kösters, 2004; Kösters et al., 2005; Kaese and Oschlies, 2000, Kaese et al., 2003 and refs. therein).

East of Faroe the DSO is paralleled by the Iceland-Scotland Overflow Water (ISOW), also enfolding ~1.4–2.4 Sv, being supplied to the North-East North Atlantic and subsequently, after having passed the Charlie Gibbs Fracture Zone, into the AMOC in the western Atlantic (Hansen and Østerhus, 2000; Sessford et al., 2019; Biastoch et al., 2021).

Important characteristics of modern DSO waters are low bottom water temperatures near −1 °C, high bottom water salinities of 34.9 psμ, and densities (σ) of 27.8–28.05 kg/m^3 for Theta = 2 °C at the bottle neck of the Denmark Strait (Whitehead et al., 1974; Macrander et al., 2007; Haine, 2021). A slight but persistent north-south density gradient is indicated for the Last Glacial Maximum (LGM, 19–23 thousand calibrated years before the year 1950; cal. ka) by $\delta^{18}O$ records of single specimens of epibenthic foraminifera (Millo et al., 2006). Also, a north-south flow path is suggested by the LGM distribution pattern of Nd isotopes, a tracer of water mass origin either flowing over continental or basaltic sediments (Blaser et al., 2020; Larkin et al., 2022).

To monitor short-term variations in the DSO over peak glacial-to-early deglacial climate change 22–15 cal. ka we now employ, partly refine, and supplement published centennial-scale proxy records obtained from sediment Core PS2644 (Fig. 1). Its high sedimentation rates enable us to derive short-term changes in surface and deep-water circulation with 20–100/200-yr resolution, a record hardly affected by bioturbational mixing (<2 cm; Trauth et al., 1997), since the local flux of planktic carbon is very low. This site marks the southern margin of the Blosseville Basin forming the northern funnel to the Denmark Strait north of westernmost Iceland (Voelker, 1999; Millo et al., 2006). Here, we compare the effect and origin of long-term climate trends and intermittent centennial-to-millennial-scale episodes of major cold spells with episodes of fast climate warming, regimes in part lasting until today. The very last major Greenland stadial we redefined and subdivided into Heinrich Stadial 1a and b (HS-1a and b), in contrast to a redefinition of stadials proposed by Andrews and Voelker (2018). Based on advanced age control (details are given below) our definition of HS-1 somewhat differs from that of Hodell et al. (2017) interpreting sediment records from the southern subpolar North Atlantic.

Moreover, we compare our records with proxy data and circulation models of stadial and interstadial analogue variations over Marine Isotope Stage 3 (MIS3) near to the northern entrance of the Denmark Strait as proposed by Hagen and Hald (2002), Sadatzki et al., and Sessford et al. (2018, 2019). The latter authors report on distinct changes in MIS3 bottom water temperature, which we now try to reproduce for late MIS2. Sessford et al. (2019) proposed stadial pathways of brine water-induced intermediate waters that finally might have been funneled into the DSO, assuming a water column homogenous in the Nordic Seas down to 1500 m.

We test this model by means of a number of multiproxy records from Site PS2644, compared to pertinent records obtained from outside on the basis of centennial-scale age resolution (Sarnthein et al., 2020): (i) We employ records from two neighbor sites at the western margin of the Vøring Plateau in the eastern Nordic Seas (Fig. 1; GIK23074 and MD95-211), where brine water formation is widely accepted to have occurred during HS-1 (Meland et al., 2008; Waelbroeck et al., 2011). (ii) We compare coeval paleoceanographic records obtained south of Iceland in the northern North Atlantic (Thornalley et al., 2011; Millo et al., 2006; Sarnthein et al., 1994).

In this way we encompass on minor and major changes in the origin of early deglacial DSO waters and related changes in the flow geometry

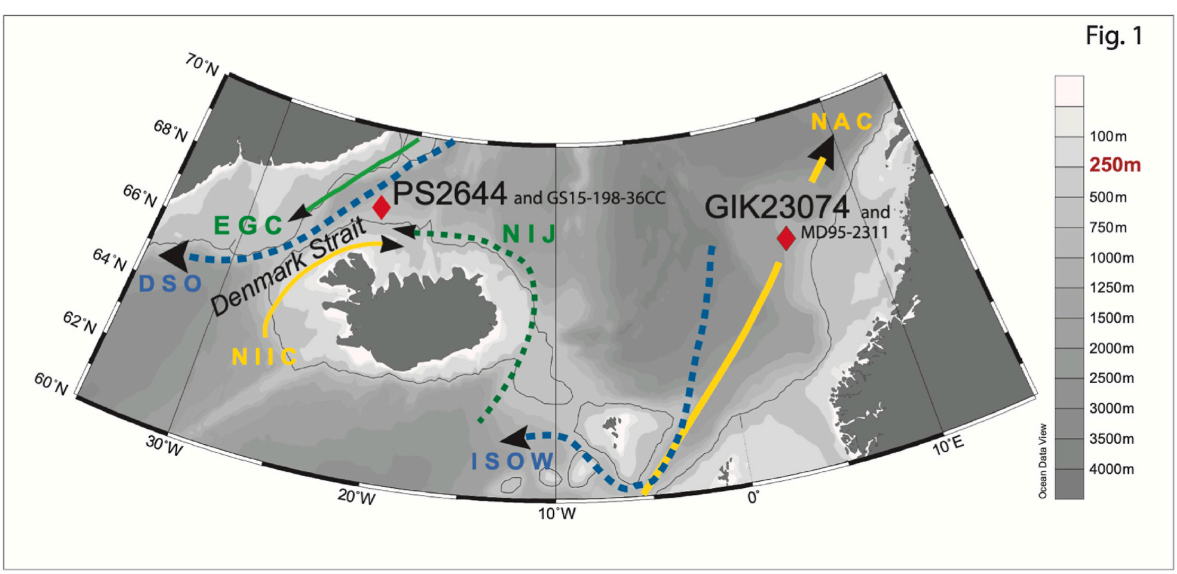

Fig. 1. Location of twin sites PS2644 and GS15-198-36 GC in the Icelandic Sea (67°52′N, 21°46′W, 777 m w.d.) and twin sites GIK23074 and MD95-2311 in the Norwegian Sea (66°40′N, 4°54′E, 1157 m w.d.). Yellow arrows mark warm surface water currents entering the Nordic Seas (NAC: North Atlantic Current, NIIC: North Iceland Irminger Current), green arrow shows the East Greenland Current (EGC). Arrows on top of broken lines depict intermediate-water currents such as the Denmark Strait Overflow (DSO), the North Iceland Jet (NIJ), during HS-1 and the Iceland Scotland Overflow Water (ISO). Bathymetry based on Ocean Data View (Schlitzer, 2002), highlighted by faint 250-m isoline. (For interpretation of the references to color in this figure legend, the reader is referred to the Web version of this article.)

of the eastern Nordic Seas and of North Atlantic intermediate- and deep-water circulation. Changes in flow geometry were possibly linked to crucial tipping points in the composition of DSO waters, items to be constrained in this study. The origin of these changes appears highly important for a better understanding of past and future trends of the "Nordic Heat Pump" and European climate change (*sensu* Jansen et al., 2020; Ditlevsen and Ditlevsen, 2023).

1.1. Oceanographic Setting of sites PS2644 and GIK23074

At Site PS2644 we trace back the composition of DSO over last glacial and early deglacial times 22–15 cal. ka. The bathymetry and modern patterns of surface and bottom water circulation in the Denmark Strait (today: ~630 m water depth; Fig. 1) are shown by Kösters et al. (2005). Macrander et al. (2007) detailed the modern DSO structure being ruled by geostrophic forcing. Site PS2644 lies at 777 m water depth, that is within the lower portion of the modern plume funneled into the DSO (Kaese et al., 2003). Prior to entering Denmark Strait, Norwegian Sea Deep Water (NSDW) today is entrained from both the Greenland Basin and Arctic Ocean (Brakstad et al., 2023).

Sediments of Core PS2644 are well suited to monitor past glacial-to-early deglacial variations in the flow of surface and deep-water masses since the site lies close to the Polar Front, that is the mean position of the border of perennial sea ice, the boundary between the East Iceland Current (EIC) and the nearshore North Iceland Irminger Current (NIIC) (Fig. 1; Voelker, 1999), while not lying too close to the Denmark Strait where extreme winnowing due to strong bottom currents largely prevents sediment deposition. To achieve an undisturbed and largely continuous sediment record of past changes in the geometry of ocean water masses, Site PS2644 was chosen on top of a narrow hemipelagic sediment ridge carefully surveyed by means of a high-resolution PARASOUND parametric echosounder system (Hubberten, 1995). Accordingly, Site PS2644 records a sediment drift free from lateral near-bottom sediment input like sediment slumps and/or turbidity currents (details in Voelker, 1999) (Fig. 2a; Fig. S1).

Core GIK23074 was retrieved from the western margin of the Vøring Plateau right below the warm North Atlantic Current (NAC), but far away from the Norwegian margin (Fig. 1; Voelker, 1999). The site is marked by exceptionally high, yet undisturbed hemipelagic sedimentation rates (25–60 cm/ky; Fig. 2b), thus providing a unique high-resolution (17–50 yr per cm sediment depth) record of ocean history in the eastern Nordic Seas at 1157 m water depth.

2. Methods: Age control and derivation of oceanographic proxy data

Precise age control of marine sediment records PS2644 and GIK23074 is essential for this study of connections between DSO, AMOC, the 'Nordic Heat Pump', and Northern Hemisphere climate. Initially, age control of Voelker (1999) was based on a high-resolution suite of planktic ^{14}C ages (Table 1), then using a constant hypothetical Marine Reservoir Age (MRA) of 400 yr for age conversion (Voelker, 1999; Voelker et al., 1998). This dating was refined by diverse correlation tie points between distinct features in the high-resolution planktic δ^{18}O records and the Greenland GISP2 δ^{18}O ice core (Fig. S1).

In the present study, however, this 'conventional' approach to obtain cal. age estimates was subject to major revision after basing the age model on the technique of ^{14}C plateau tuning (Fig. 2a and b) (Sarnthein et al., 2020, 2023). Various approaches to estimate calibrated age values are listed below. Also, the Vedde volcanic ash layer (Fig. S1) was used as age tie point at ~10.31 ± 0.05 ^{14}C ka (=12.1 cal. ka), based on analyses of ambient land plant macrofossils (age revised by Birks et al., 2017; age conversion of Bronk Ramsey et al., 2020).

The derivation and constraints of paleoceanographic proxy values and radiogenic isotopes employed in this study are summarized in Supplementary Text no. 1. In particular, distinct variations in % *Neogloboquadrina pachyderma* sin (Nps; in "old" terminology) served as tracer of short-term changes in sea surface temperature (SST). In turn, these features served as stratigraphic age markers to investigate the possibly coeval character of temperature changes recorded by δ^{18}O oscillations in Greenland ice core record GISP2, where 'genuine' cal. ages are based on an incremental time scale (Grootes and Stuiver, 1997; Svensson et al., 2008) (Fig. S1; Voelker, 1999).

To provide an independent time scale on top of the conventional stratigraphic alignment of planktic ^{14}C ages, we refined the ^{14}C-based age control by defining local planktic ^{14}C age plateaus and plateau boundaries being tuned as cal. age tie points to pertinent age-calibrated structures in the atmospheric ^{14}C record of Lake Suigetsu (Table 1; Sarnthein et al., 2023). In turn, Suigetsu age control was based on U/Th-based model ages of Bronk Ramsey et al. (2020) (details of age derivation in Sarnthein et al., 2020, 2023) (Fig. 2a and b). We are aware that this approach has been challenged by Bard and Heaton (2021). However, we suggest that ^{14}C plateau tuning (PT) produces trustworthy age models for a series of reasons: (i) It has clearly been shown that past centennial to millennial-scale fluctuations of the Suigetsu atmospheric ^{14}C record have been authentic (Sarnthein et al., 2023). (ii) Our technique of plateau tuning solely relies on the tuning of a whole suite of ^{14}C plateaus in the atmosphere and a sediment record each (Fig. 2a and b), thus can clearly distinguish and/or exclude potential fake plateaus in a sediment core, such as given for the top section of HS-1 in Core GIK23074 (Fig. 2b). (iii) We demonstrate prominent cases of abrupt deglacial climate change during LGM and HS-1 near 21.9, 18.4, and 16.2 cal. ka, where the age estimates for hydrologic changes based on ^{14}C-plateau tuning precisely match pertinent ages based on incremental age counts in ice core NGRIP with <100 years deviation (Table 2; Figs. 3 and 4). This fit is far from incidental, but not revealed by any conventional ^{14}C-based stratigraphic method. Since the records PS2644 and GIK23074 are related to considerations of oceanic and atmospheric circulation, and heat transport, the agreement makes sense in a coupled ocean-atmosphere climate system.

Calendar-age uncertainties of the atmospheric ^{14}C plateau boundaries employed for our tuning approach hardly exceed ±100 – ±250 yr each (1σ; Sarnthein et al., 2020; 2023). This allows a detailed comparison of AMOC and atmospheric climate fluctuations depicted in Greenland ice cores. Local MRA of planktic foraminifers/surface waters were deduced from the age difference between the average ^{14}C age estimates of paired, thus coeval atmospheric and marine ^{14}C plateaus based on plateau tuning (Sarnthein et al., 2020; and refs. therein). Benthic ventilation ages were deduced as explained in Suppl. Text no. 1.

Also, a Th/U-based benthic cal. age was obtained from a solitary coral in Core MD95-2011 (66°58′18N; 07°38′36E; 1048 m depth; samples 1211-D, -S, -M, and -K), like Site GIK23074 a site below the warm North Atlantic Current. The ratio of thorium to uranium which yields the calendar age of the coral, was measured by thermal ionisation mass spectrometry (TIMS) at Heidelberger Akademie der Wissenschaften (Heidelberg, Germany) according to methods outlined by Bollhöffer et al. (1996) and Neff et al. (1999). The Th/U isochrone age of 16.1 ± 0.8 ka was compared with uncorrected ^{14}C ages of 15.5–15.7 ± 0.1 ka for specimens of planktic Nps (samples KIA3519, KIA6450, KIA4599) sampled right below and above the coral. The Th/U-based cal. age is compatible with the fast changes of planktic cal. age, given paired MRA of 500–1000 yr derived from ^{14}C plateau tuning of planktic ^{14}C ages at Site GIK23074 (Fig. 3) (Dreger, unpubl. comm. 2000; Th/U data of Lomitschka and Mangini, 1999).

Sedimentation rates of 5–25 cm/ka and 25–46 cm/ka were derived for each ^{14}C plateau from the age interpolation of sediment sections using the cal. age of planktic ^{14}C plateau boundaries (Fig. 2a and b). The estimates were widely supported by ages obtained from linear age interpolation between conventional age tie points to pertinent ages of ice core record GISP2 (Voelker, 1999; Fig. S1).

Core PS2644 largely lacks modern and Holocene reference values for most proxy records employed in this study. Except for a few cm thick

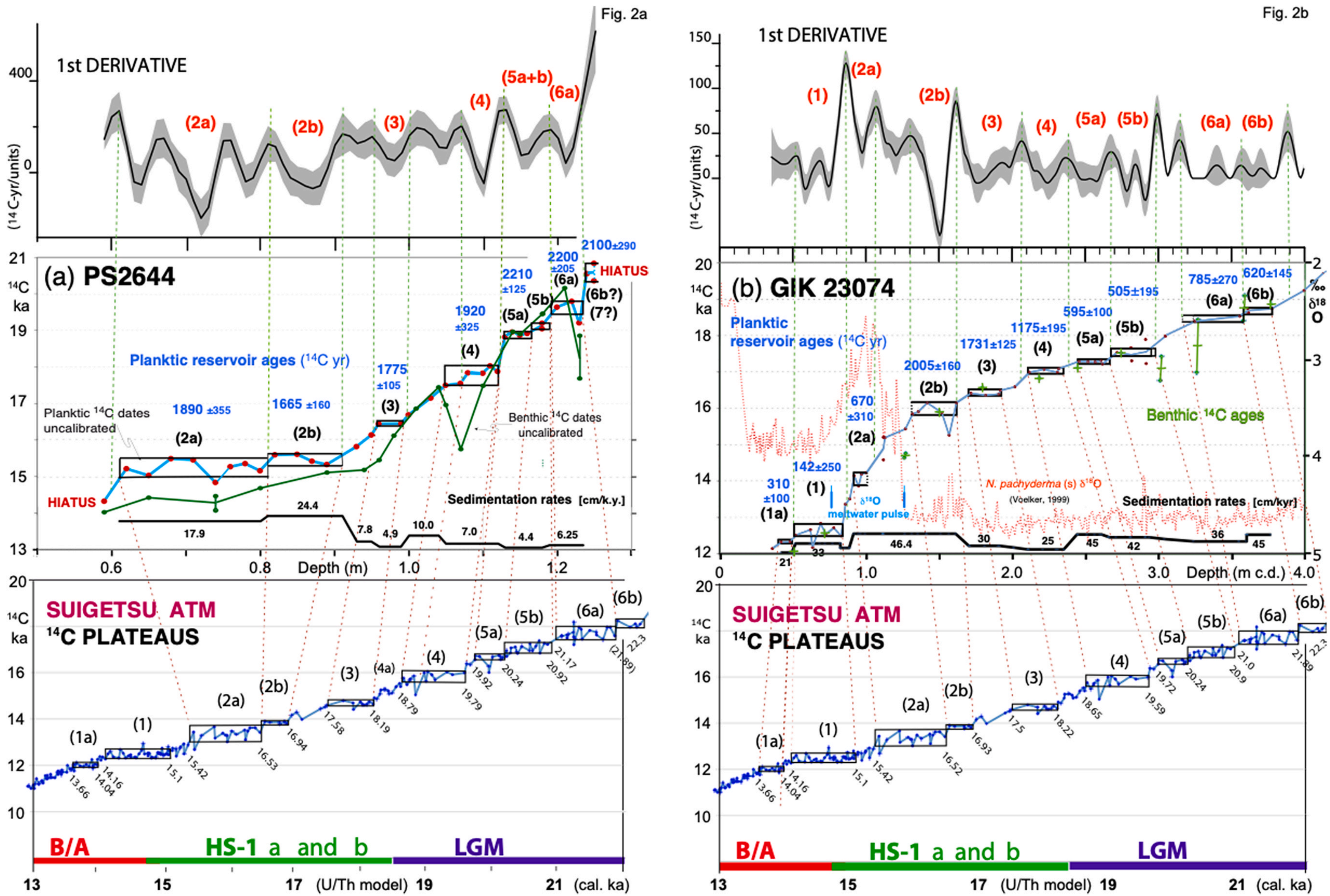

Fig. 2. a and b. Planktic ^{14}C records of sediment cores PS2644 and GIK232074 plotted vs. core depth; for core locations see Fig. 1. Local planktic reservoir ages (in blue) reflect the difference between the average raw ^{14}C age of planktic ^{14}C plateaus measured in a core and the average ^{14}C age of equivalent atmospheric (atm) ^{14}C plateaus at Lake Suigetsu (Bronk Ramsey et al., 2020) (horizontal boxes, numbers 1–6 in brackets). Ages of plateau boundaries of atm record are given in cal. kyr BP (before 1950 AD). Note atmospheric plateau 4a (lowermost panel in Fig. 2a) that covers a basic switch in DSO flow geometry at Site PS2644 ~18.6–18.4 cal. ka, as reflected by a coeval incursion of fairly young and warm bottom waters during ^{14}C plateau 4, right at the onset of HS-1b (panels 1 and 3 in Fig. 4). Top panel shows units of the 1st derivative (^{14}C yr per m core depth) and 1-σ uncertainty range, with peaks indicating ^{14}C jumps in between ^{14}C plateaus numbered in red, as defined in Sarnthein et al. (2023). Green dots display paired benthic ^{14}C ages. B/A = Bølling-Allerød; HS-1a + b = Heinrich Stadial 1 a and b; LGM = Last Glacial Maximum. In both cores sedimentation rates are deduced from the cal. age range of nearby ^{14}C plateau boundaries. Red dotted line in Fig. 2b shows local planktic δ^{18}O record of *N. pachyderma* sin. (Voelker, 1999). (For interpretation of the references to color in this figure legend, the reader is referred to the Web version of this article.)

Table. 1a
PS2644 All ^{14}C data vs. Suigetsu atm. U/Th model ages.

PS 2644-5		67°52′N, 21°46′W, 777 m w.d.)				15–22 cal. ka						
Labcode	**Midpoint Core Depth** (cm)	**Raw Planktic ^{14}C age** *(N. pachyderma s)* (yr BP) (revised 2011)	**Error (1s) (±yr)**	**SUIGETSU Plateau no. top/base**	**Cal. ages tuned to SUIGETSU U-Th model ages (kyr BP) BOLD: Plateau bound. ages**	**Sedim. Rate cm/ky _yr/cm**	**MRA-Planktic Res. Age vs. Suigetsu** (^{14}C yr)	**Labcode**	**Raw Benthic ^{14}C age** *Cibi. wuell.* (yr BP)	**Error (1s) (±yr)**	**Benthic-Planktic Age Difference** (^{14}C yr)	**r a w Benthic Vent. Age** vs. Suigetsu (^{14}C yr)
HIATUS												
KIA 802	59	14366	75		15305		1890	KIA 741	14049	82	−315	1575
	61	–		**2a top**	**15415**	**17.94**	1890					
KIA 29415	62	15260	75	2a	15471	_55.7	1890					
KIA 77	65	15081	162	2a	15638		1890	KIA 1649	14450	80	−630	1210
KIA 29416	68	15540	90	2a	15805		1890					
KIA 29417	71	15510	80	2a	15972		1890					
KIA 736	74	14887	116	2a	16140		1890	KIA 742	14131	82	−750	1090
KIA 743	74	–		2a	16140		1890	KIA 743	14494	89	−390	1450
KIA 29418	76	15320	75	2a	16251		1890					
KIA 29419	78	15405	75	2a	16363		1890					
KIA 78	80	15212	195	2a	16474		1890	KIA 1650	14720	90	−490	1350
	81	–		**2a/2b**	**16530**	**24.39**	1890					
KIA 29347	82	15640	70	2b	16571	_41	1665					
KIA 79	85	15659	160	2b	16694		1665					
KIA 29420	87	15470	75	2b	16776		1665					
KIA 737	89	15375	121	2b	16899		1665	KIA 744	15150	90	−230	1400
	91	–		**2b base**	**16940**	**7.81**	1665					
KIA 29404	93	15870	70		17196	_128						
KIA 43118	94	–			17324			KIA 43118	15170	95	−700	960
KIA 41438	95	16140	100		17452							
KIA 29256	96	16500	85	**3 top**	**17580**	**4.92**	1775	KIA 43119	15440	90	−1060	715
KIA 45817	98	–		3	17986	_203	1775	KIA 45817	16110	85	−390	1380
KIA 803	99	16507	90	**3 base**	**18190**	**10**	1775					
KIA 41997	100	16690	100		18290	_100	1775					
KIA 45818	101	–			18390		1775	KIA 45818	16850	100	90	1800
KIA 29346	103	17210	80		18590							
KIA 43662	104	–			18690		1920	KIA 43662	17435	110	0	1920
KIA 41284	105	17500	100	**4 top**	**18790**	**7**	1920	KIA 44984	16950	100	−550	1370
KIA 804	107	17618	113	4	19076	_143	1920	KIA 1641	15790	120	−1810	90
KIA 1641	107	–		4	19076		1920				−1530	390
KIA 41998	108	17840	110	4	19219		1920					
KIA 41285	108	18850	110	4	19219		1920					
KIA 29421	110	17900	100	4	19505		1920	KIA 43663	17480	110	−420	1500
KIA 41286	111	18030	100	4	19648		1920					
KIA 41287	112	17880	120	**4 base**	**19790**		1920					
KIA 41999	113	18820	125	**5a top**	**19920**	**9.4**	2210					

(*continued on next page*)

Table. 1a (*continued*)

PS 2644-5		67°52′N, 21°46′W, 777 m w.d.				15–22 cal. ka						
Labcode	**Midpoint Core Depth** (cm)	**Raw Planktic ^{14}C age** *(N. pachyderma s)* (yr BP) (revised 2011)	**Error (1s) (±yr)**	**SUIGETSU Plateau no. top/base**	**Cal. ages tuned to SUIGETSU U-Th model ages (kyr BP) BOLD: Plateau bound. ages**	**Sedim. Rate cm/ky _yr/cm**	**MRA-Planktic Res. Age vs. Suigetsu** (^{14}C yr)	**Labcode**	**Raw Benthic ^{14}C age** *Cibi. wuell.* (yr BP)	**Error (1s) (±yr)**	**Benthic-Planktic Age Difference** (^{14}C yr)	**r a w Benthic Vent. Age** vs. Suigetsu (^{14}C yr)
KIA 41288	114	18810	110	5a	20026	_106	2210	KIA 43120	17480	110	−20	2190
KIA 42000	114	18980	130	5a	20026		2210					
KIA 805	115	18952	129	5a	20132		2210	KIA 43121	18900	120	−50	2160
KIA 29254	116	19000	110	**5a base**	**20240**	**4.4**	2210					
KIA 29405	118	19130	90	5b ?	20694	_227	2200	KIA 43664	19450	130	320	2520
KIA 29572	118	19280	135	5b ?	20694		2200				170	2370
	119	–		**6a top**	**21170**	**6.25**	2100					
KIA 80	120	19727	245	6a	21330	_160	2100				430	2530
KIA 43665	121	–		6a	21490		2100	KIA 43665	20160	140		
KIA 29345	122	19890	100	6a	21650		2100				270	2370
KIA 806	123	19288	126	6a	21810		2100	KIA 745	17740	160	−360	1740
KIA 806	123	19210		6a	21810		2100	KIA 44986	18850	265	−1530	570
	123.5	–		**6a base**	**21890**		2100					
KIA 42001	124	20605	145	6b ?	21970							
KIA 29344	125	20460	110	6b ?								
KIA 29571	125	20940	165	6b ?								
	HIATUS	–			**~22000**							

AMS ^{14}C ages of planktic and benthic samples were measured at the Leibniz Laboratory, University of Kiel (KIA numbers).
DATA SOURCES
Voelker (1999), supplemented by benthic ^{14}C datings of Sarnthein et al. (2015).
This study: Conversion of planktic ^{14}C dates to cal. age estimates tuned to SUIGETSU-U/Th-based model ages (Bronk Ramsey et al., 2020).

sediment layer ^{14}C-dated to −0.18 and −0.23 ka (unconverted), that forms the actual core top, a strong DSO flow has hindered any Holocene sediment deposition and/or led to sediment erosion prevalent over most of the last ~15 cal. ka (Voelker, 1999; Kuijpers et al., 2003).

3. Results: four time slices ~22–15 cal. ka (Table 2)

Core PS2644 contains a sediment section of LGM and HS-1 times, that starts and ends with major stratigraphic gaps prior to ~21.8 cal. ka and after ~15.1 cal. ka (Fig. 2a), that is, near the end of Greenland Interstadial (GI) 2 and close to the end of HS1. The subsequent Bølling-Allerød (B/A) interstadial was lost by erosion and/or non-deposition (Fig. S1; Voelker, 1999; Voelker et al., 2000). Probably this was a result of enhanced sediment winnowing, when an enhanced DSO was constricted near the northern entrance of the Denmark Strait. X-ray radiography shows that the hiatus forms a distinct unconformity at 54-53 cm composite depth (c.d.), right below the Vedde Ash layer at 52 cm c.d., 12.1 cal. ka (Voelker, 1999; Voelker and Haflidason, 2015).

This peak-glacial-to-early-deglacial sediment record of PS2644 for MIS2 is partitioned into four stratigraphic time slices I to IV (Table 2). They give a joint record of changes in epibenthic ventilation ages and stable C and O isotope records of planktic and epibenthic foraminifers (Nps and *Cibicidoides lobatulus*), and less distinct, in planktic MRA. Also, the partitioning is reflected by Nd and Pb isotope records, moreover, by distinct changes in sedimentation rate (Figs. 4 and 5). The time slices likewise apply to the suite of past ocean changes depicted in the proxy records of both cores PS2644 and GIK23074.

Time slice (I), 21.8–19.8 cal. ka, in PS2644 covers the top portion of the Last Glacial Maximum (LGM; defined by Mix et al., 2001). During slices I and II, sea ice-covered subsurface waters of the East Greenland Current (EGC) at PS2644 (Sadatzki et al.,) are marked by minimum temperature and peak salinity values as reflected by fairly persistent planktic δ^{18}O values of 4.5 ‰ and SST of 3.7 °C based on census counts of planktic foraminifera species (Pflaumann et al., 2003; Millo et al., 2006). Time slice I shows maximum MRA of 2200 yr, after 19.8 cal. ka dropping to ~1900 yr (Fig. 4).

During time slice I, bottom waters at PS2644 were marked by a bipartite population of epibenthic δ^{13}C values. One of them presents the highest δ^{13}C values and, despite all processes of ocean mixing, the highest deep-water ventilation recorded in the global ocean (Millo et al., 2006; Duplessy et al., 2002), indicative of Arctic sources, clearly predominant over 21.8–20.3 cal. ka, when bottom water ventilation ages reached up to 2500 ^{14}C yr.

Radiogenic isotopes in the detrital sediment fraction indicate a mixture of Arctic and European sources of the sediment, with a modest contribution from nearby Iceland (Figs. 4 and 5; Struve et al., 2019; Larkin et al., 2022; Blaser et al., 2016). Possibly this could have been caused by the complete glaciation of Iceland and/or a change in ocean currents shielding the site from Icelandic input. The authigenic sediment fraction shows significantly more radiogenic signatures in both Nd and

Table. 1b
GIK23074 All ^{14}C data vs. Suigetsu atm. U/Th model ages.

GIK 23074		**66°40′N, 4°54′E, 1157 m w.d.**				**13–22.3 cal. ka**							
Labcode	**Midpoint Depth** (cm)	**Raw Plankt. ^{14}C Age** (N. pachyderma s) (kyr BP)	**Error (1s) (±yr)**	**SUIGETSU Plateau No.**	**MRA_Planktic Res. Age vs. Suigetsu** (14C yr)	**Cal. ages tuned to SUIGETSUU-Th model ages (kyr BP)**	**Sedim.rate cm/ky** _yr/ cm (corr. 2023)	**Labcode**	**Midpoint Depth** (cm)	**Raw Benthic^{14}C Date** (C. teretis)	**Error (1s) (±yr)**	**Benthic-Planktic Age Difference** (^{14}C yr)	**Benthic Vent. Age** (yr) vs. Suigetsu
KIA 705	35.5	12130	70		320	13368							
KIA 40194	41.5	12310	80	1a	320	**13656**	18.83						
KIA 1438	47.5	12320	70	1a	320	13921	_53						
	49.5	–		1a/1 top	320	14065		UCI 196253	50.75	12070	180	−370	50
KIA 40195	51.5	12500	80	1	210	**14187**	36.13		51.5				
KIA 40196	61.5	12650	90	1	210	14464	_27.7						
KIA 41666	63.0	**12160**	100	1	210	14506							
KIA 1439	68.5	12820	70	1	210	14658							
KIA 41667	72.0	12530	95	1	210	14755		AWI 1262.1.1	71.5	12,560	45	−55	155
KIA 41668	77.5	**12700**	90	1	210	14907							
KIA 41669	82.5	**12480**	100	1 base	210	**15045**	26.1						
KIA 40898	85.5	13350	90			14160	_38.3						
KIA 40899	88.5	13500	90			14275							
KIA 40197	91.5	14130	90	2a top	685	**15420**	46.35						
KIA 1440	94.5	13850	70	2a	685	15485	_21.6						
KIA 40900	96.5	14180	100	2a	685	15527							
KIA 41670	99.5	**14220**	90	2a	685	15593							
KIA 40198	111.5	15190	100	disturbed									
KIA 41672	111.5	**14570**	120										
KIA 899	112.5	15180	100			assumed							
KIA 40902	126.5	15420	120	disturbed		16530		UCI 196123	126.4	14,700	60	−1100	1035
KIA 40199	131.5	15830	100	2b	2135	16638							
KIA 1441	135.5	15900	80	2b	2135	16724							
KIA 40200	141.5	16140	110	2b	2135	16854							
KIA 40201	151.5	15870	110	2b	2135	16722		AWI 1263.1.1	150	15,900	30	45	2180

(*continued on next page*)

Table. 1b (*continued*)

GIK 23074		66°40′N, 4°54′E, 1157 m w.d.				13–22.3 cal. ka							
Labcode	**Midpoint Depth** (cm)	**Raw Plankt. ^{14}C Age** (N. pachyderma s) (kyr BP)	**Error (1s) (±yr)**	**SUIGETSU Plateau No.**	**MRA_Planktic Res. Age vs. Suigetsu** (14C yr)	**Cal. ages tuned to SUIGETSUU-Th model ages (kyr BP)**	**Sedim.rate cm/ky** _yr/ cm (corr. 2023)	**Labcode**	**Midpoint Depth** (cm)	**Raw Benthic^{14}C Date** (C. teretis)	**Error (1s) (±yr)**	**Benthic-Planktic Age Difference** (^{14}C yr)	**Benthic Vent. Age** (yr) vs. Suigetsu
KIA 1442	156.5	15250	100	2b	2135	16830							
KIA 40202	161.5	16140	120	2b base	2135	16940							
	170.5	–		3 top	1925	**17580**	33.47						
KIA 40203	171.5	16400	110	3	1925	17610	_29.8						
KIA 40204	181.5	16350	110	3	1925	17908		AWI 1264.1.1	179.5	16,575	30	170	2095
KIA 900	190.5	16380	110	3	1925								
KIA 40205	191.5	16480	120	3 base	1925	18205							
KIA 40206	201.5	16580	110										
	211.0	–		4 top	1150	**18790**	27.7						
KIA 40207	211.5	16980	120	4	1150	18826	_36						
KIA 40208	221.5	17060	120	4	1150	19170		AWI 1265.1.1	218.5	16,835	30	−190	960
KIA 901	230.5	16980		4	1150	19494							
KIA 40209	231.5	17080	120	4	1150	18530							
	235.5	–		4 base	1150	19790			235.5				
	244.5	–		5a top	675	19920	68.8	UCI 196124	243.75	17080	70	−200	475
KIA 902	245.5	17280	110	5a	675	19934	_14.5						
KIA 40258	251.5	17270	80	5a	675	20021							
KIA 903	256.5	17260	120	5a	675	20094							
KIA 40259	260.5	17300	90	5a	675	20152							
KIA 40260	261.5	17210	85	5a	675	20167							
	266.5	–		5a/b	675	**20240**	41.67		266.5				
KIA 40261	271.5	17520	80	5b	470	20360	_24	UCI 196125	274.75	17490	150	−30	440
KIA 41673	281.0	**17650**	105	5b	470	20588							
KIA 41676	281.5	**17295**	125	5b	470	20600							
KIA 41674	291.0	**17880**	105	5b	470	20828							
KIA 41677	291.5	**17220**	115	5b	470	20840							
	294.0	–		5b base	470	**20900**	179.4		294.0				
KIA 904	304.5	17970	115			20958	_5.6	UCI 191624	301.5	17100	330	−870	−110
KIA 1443	324.5	**18380**	110	6a top	760	**21070**	36	UCI 191625	326.5	17720	730	−660	100
KIA 905	355.5	**18520**	125	6a	760	21941	_27.8						

(*continued on next page*)

Table. 1b (*continued*)

GIK 23074		66°40′N, 4°54′E, 1157 m w.d.				13–22.3 cal. ka							
Labcode	**Midpoint Depth** (cm)	**Raw Plankt. ^{14}C Age** (N. pachyderma s) (kyr BP)	**Error (1s) (±yr)**	**SUIGETSU Plateau No.**	**MRA_Planktic Res. Age vs. Suigetsu** (14C yr)	**Cal. ages tuned to SUIGETSUU-Th model ages (kyr BP)**	**Sedim.rate cm/ky _yr/cm** (corr. 2023)	**Labcode**	**Midpoint Depth** (cm)	**Raw Benthic^{14}C Date** (C. teretis)	**Error (1s) (±yr)**	**Benthic-Planktic Age Difference (^{14}C yr)**	**Benthic Vent. Age** (yr) vs. Suigetsu
	360.5	–		6a/b	760	**22080**	77.3	UCI 191626	358.5	18760	350	240	520
KIA 41675	361.0	18730	130	6b	580	22087	_13						
KIA 41678	361.5	18620	110	6b	580	22100							
KIA 906	377.5	18730	125	6b base	580	22300		AWI 1266.1.1	377	18,875	25	145	435
KIA 907	399.5	19230	140										
KIA 908	412.5	19670	150										
KIA 909	422.5	19940	140										

AMS ^{14}C ages of planktic and benthic samples were measured at the Leibniz Laboratory, University of Kiel (KIA numbers), the AWI AMS facility in Bremerhaven (AWI numbers) and the Keck Carbon Cycle AMS facility (UCI numbers), University of California, Irvine.
DATA SOURCES
Planktic ^{14}C ages of Voelker (1999), supplemented by ^{14}C dates of Sarnthein et al. (2015).
PLUS: Conversion to cal. age estimates tuned to IntCal20 and SUIGETSU-U/Th-based model ages (Bronk Ramsey et al., 2020).
Benthic ^{14}C ages: This study.

Pb than the detrital fraction (Table 3). A similar effect was found in front of the Barents Shelf (Struve et al., 2019) and in the eastern subpolar North Atlantic (ODP980; Crocket et al., 2013), attributed to glacial erosion of terrestrial metal oxides in N.W. Europe and their supply to the ocean.

Time slice (II) 19.8–18.4 cal. ka already reflects the end of the LGM, as suggested by an initial major deglacial rise in eustatic sea level starting at 19.4 cal. ka (atmospheric ^{14}C ages of Hanebuth et al., 2009). After 19.8 cal. ka, the antecedent high in bottom water ventilation age was short-term replaced by very low ages of 100–400 yr. North of Iceland they mark an early deglacial inflow of bottom waters reflecting a direct contact with the atmosphere nearby, like the inflow at the end of Greenland Interstadial (GI 2). Most important, the young bottom water ages at site PS2644 resemble LGM ages found at Site GIK23074 in the eastern Nordic Seas. Moreover, we find a distinct rise in detrital radiogenic εNd values (= deviation of Nd isotopic composition from that of chondrites) up to −5, which traces an increased contribution by Icelandic basalts passed by DSO waters prior to reaching Site PS2644 (Fig. 4), or increased supply through an early deglaciation of parts of Iceland (*sensu* Crocket et al., 2013).

Time slice III, 18.4–17.2 cal. ka, reflects a phase of transition, when planktic δ^{18}O values at PS2644 dropped gradually by more than 1.5 per mil (Fig. 4). The drop likely reflects a drop in sea surface salinity (SSS) induced by meltwaters advected from southwest, from the Irminger Sea, thereby recording the onset of HS-1. Also, foraminifera census counts reflect a SST rise up to 4 °C (Sarnthein et al., 2001). Local MRA then dropped to 1670–1780 yr, a value slightly lower than before, but still reflecting a reduced carbon exchange of sub-surface waters with the atmosphere, attenuated by ongoing perennial sea ice cover. At eastern Site GIK23074 the onset of time slice III/HS-1 was marked by an impressive sudden rise of MRAs from 1175 to 1900 yr, a level higher than the coeval level at western Site PS2644 (Fig. 2b and 3).

Like surface waters, bottom waters at Site PS2644 reveal a major change near 18.4 cal. ka: Maxima of benthic δ^{18}O values measured on single epibenthic specimens show an abrupt, centennial-scale ^{18}O depletion by 0.8 ‰, by theory equivalent to a 3.4 °C rise in bottom water temperature (Fig. 4). At that time, extremely high epibenthic δ^{13}C values of the LGM were replaced by medium high values, which went along with a renewed short-term drop in bottom water ventilation ages down to 750 yr near 17.5 cal. ka.

εNd both in the detrital and authigenic fractions have further increased, indicating an elevated supply of Icelandic volcanogenic material overflown by DSO waters prior to reaching Site PS2644 (Fig. 4) or a direct input by surface currents such as the North Iceland Irminger Current (Fig. 1). Contemporaneous ratios of authigenic ^{206}Pb/^{204}Pb show a pronounced short-lasting maximum (Fig. 5) that could result from an increased supply of Pb glacially eroded from N.W. Europe 18.4–17.0 cal. ka.

Time slice IV, 17.2–15.1 cal. ka, records a matured sea ice-covered meltwater regime at Site PS2644 (persistent planktic δ^{18}O minimum in Fig. 4) during HS-1, lasting until the onset of a hiatus. Near its onset, the time slice was marked by an SST peak of 7.5 °C (deduced by census counts of planktic foraminifera species; Voelker, 1999). MRA continued near 1900 yr as in slice III. Also, paired bottom water ages continued at 1100 to 1550 ^{14}C years, that is significantly lower than during the LGM. Epibenthic δ^{13}C values of bottom water ventilation were as low as 0.6–1.4 ‰ (Fig. 4).

At the onset of time slice IV, bulk sedimentation rates at Site PS2644 show a major sudden rise, almost by a factor of three, with sediments marked by a high concentration of ice-rafted hematite-stained quartz grains originating from (North-) East Greenland (Voelker, 1999). At that time, detrital ^{206}Pb/^{204}Pb ratios have decreased, while εNd has become more radiogenic (Fig. 4), which would agree with an enhanced input of Neogene basalt sediment on the expense of the "European" source (Fig. 5). The basalt signal then may have come from the nearby Iceland-Scotland Ridge east of Iceland, overflown by the North Iceland

Table 2

Sediment core number	Events (cm)	Core depth	Comparison of cal. age estimates, by means of Correl. to GISP2 (400-yr MRA) (yr before 1950 AD) Voelker (1999)	IntCal20^{14}C yr vs. **cal. yr** (yr before 1950 AD) corr. by 400-yr MRA	**^{14}C PT**	Records of GISP2 and NGRIP (yr before 2k) (δ^{18}O GICC05)	Major features
PS2644	Vedde ash layer	52	12.12/12.3	– –	**12.1**	**11.98**	– – – – – –
PS2644	Base of hiatus	>58	– –	~13966/**16.9**	**~15.1**	**~15.1**	•GICC05: gradual d18O rise reflects onset of atm. warming on top of HS-1a
GIK23074	Start of Barents Sea meltwater outbreak	112	16.47	15020/**18.2**	**16.2**	**16.1–16.2**	•GICC05: abrupt d18O decrease shows start of HS-1a atm. temperature minimum
PS2644	Time Slice 4 - Base	93	17.8	15470/**18.8**	**17.2**	no record	•Beginning of planktic d18O minimum shows onset of deglacial meltwater maximum
PS2644	Time Slice 3 - Base	101	– –	~16600/**20.1**	**18.4**	**18.45**	•Onset of major planktic d18O decrease shows start of meltwater input at PS2644/Start of HS-1b •Drop in epibenthic d18O values shows abrupt 3.5 °C rise of DSO temperature minimum •GICC05: abrupt d18O decrease shows start of HS-1b atm. temperature minimum
PS2644		107	– –	17218/**20.8**	**19.75**	no record	•Brief minimum of benthic ventilation ages shows short-term incursion of very young DSO waters
PS2644	Time Slice 2 - Base	112–113	18.84	17480/**21.0**	**19.8**	no record	•Drop in surface water ventilation age marks end of LGM
PS2644	Time Slice 1 - Base	123	>20.3	~18550/**22.4**	**21.8**	**21.8**	•Minimum of benthic ventilation ages shows incursion of young DSO waters, near to the •Top of hiatus at Greenland Interstadial (GI) 2

Jet, when heading west for Site PS2644. Also, Fig. 5 may suggest an input of basalt debris from basalt outcrops in East Greenland south of 70°N. This source, however, is unlikely, since it would require a transport across the (sea-ice covered) frontal systems of the East Greenland Current (EGC) flowing toward southwest (Fig. 1).

At Site GIK23074, MRAs and bottom water ventilation ages (Fig. 3) reveal a suite of changes in differential stratification of the eastern Nordic Seas contemporary with those in the west, at PS2644 (Fig. 1). In addition, however, time slice IV has been dissected near 16.2 cal. ka by a subsequent major drop in both MRA and bottom water ventilation age (Fig. 2b and 3). The drops are tied to a great late-deglacial meltwater outbreak from the Barents Shelf as documented by an extreme short-term low in planktic δ^{18}O values extending far south up to the Faeroe Isles (Weinelt et al., 1991; Voelker, 1999).

4. Discussion – linkages between short-term changes in sea surface salinity, sources of DSO water, AMOC, temperature, and climate

4.1. In search for differential sources of DSO water

Today, intermediate and deep waters of the Icelandic, Greenland, and Arctic Seas form the source of DSO waters, ultimately fed by the convection of waters of North Atlantic sources (NAC) and, less important, by the subsurface North Iceland Jet (NIJ) (Fig. 1). Stable isotopes, ventilation ages, and radiogenic isotopes of waters feeding the DSO (Fig. 4) reveal past millennial-scale changes in the geometry of DSO circulation at Site PS2644, in part, supported by stables-isotope records from Site GIK23519 at the southern exit of the Denmark Strait (64°48′N, 29°36′W, 1893 m w.d.; Millo et al., 2006).

Diverse benthic ^{14}C ventilation ages back the definition of three different modes of the DSO: (1) DSO mode 1 is marked by extreme age minima both at the very end of GI 2 (Fig. 4; Table 2) and the end of the LGM between ~19.5 and 18.7 cal. ka (Mix et al., 2001), the center of time slice II (Fig. 4). (2) DSO mode 2 is earmarked by high ventilation ages of 2200–2500 yr over most of LGM time slice I, moreover, during late time slice 2, 18.7–18.4 cal. ka. (3) Finally, DSO mode 3 occurs over time slices III and IV with intermediate ventilation ages of 1100–1600 yr. It started with minimum ages of ~700–960 yr, similar to those of mode 1, and continued up the hiatus at ~15.1 cal. ka (Fig. 2a; Voelker, 1999).

DSO modes 1 and 2 are marked by two separate coeval populations of epibenthic δ^{13}C values each of them measured on single foraminifera specimens: δ^{13}C values of 0.8–1.4 ‰ are paired with values of 1.4–1.7 ‰ (encircled in Fig. 4). The latter group presents the absolute maximum of δ^{13}C-based estimates of LGM global ocean ventilation (Millo et al., 2006), also recorded at Site GIK23519 south of the Denmark Strait (Millo et al., 2006). In part, the extreme values may just form a product of seasonal to decadal variability. Also, they suggest that waters of DSO mode 2 may have come from polar regions (Brakstad et al., 2023; model results of Haine, 2021), waters largely bare of any organic carbon flux. Likewise, paired δ^{18}O values of ~5.5 ‰ for single foraminifera specimens in Core PS2644 indicate extremely low intermediate-water temperatures characteristic of Arctic source waters (Waelbroeck et al., 2011).

The end of the LGM, however, was marked by a brief pulse of DSO mode 1 (Fig. 2a and 3, Table 2). A major portion of DSO waters then has come from deep-water convection nearby, likely close to Site GIK23074 in the eastern Nordic Seas, as outlined below. Overall, the flow geometry of LGM DSO modes 1 and 2 may have come close to that of modern circulation patterns. Nd and Pb radiogenic isotope signatures confirm that the sediment discharge linked to DSO modes 1 and 2 has been largely derived from northern Europe, less from the Arctic or from basaltic sediments on the Iceland-Scotland Ridge overflown by the North Iceland Jet (Figs. 1, 4 and 5).

By comparison to the Holocene, the flow strength of DSO mode 2 was somewhat reduced as suggested by medium high sedimentation rates at PS2644 over most of time slices I–III (Fig. 4). Vice versa, the flow strength of DSO mode 1 was much enhanced. At >21.8 cal. ka, the end of GI 2, during the B/A, and major parts of the Holocene the DSO mode 1 resulted in major sedimentation gaps at Site PS2644, where the northern inflow to the DK Strait was constricted. Today, few centimeter-thick modern sediments were ^{14}C dated, hence record a return of DSO mode 2 (Voelker, 1999).

During HS-1 time slices III and IV, proxy data of DSO mode 3 strongly differ from those of DSO modes 1 and 2: A broad range of medium high

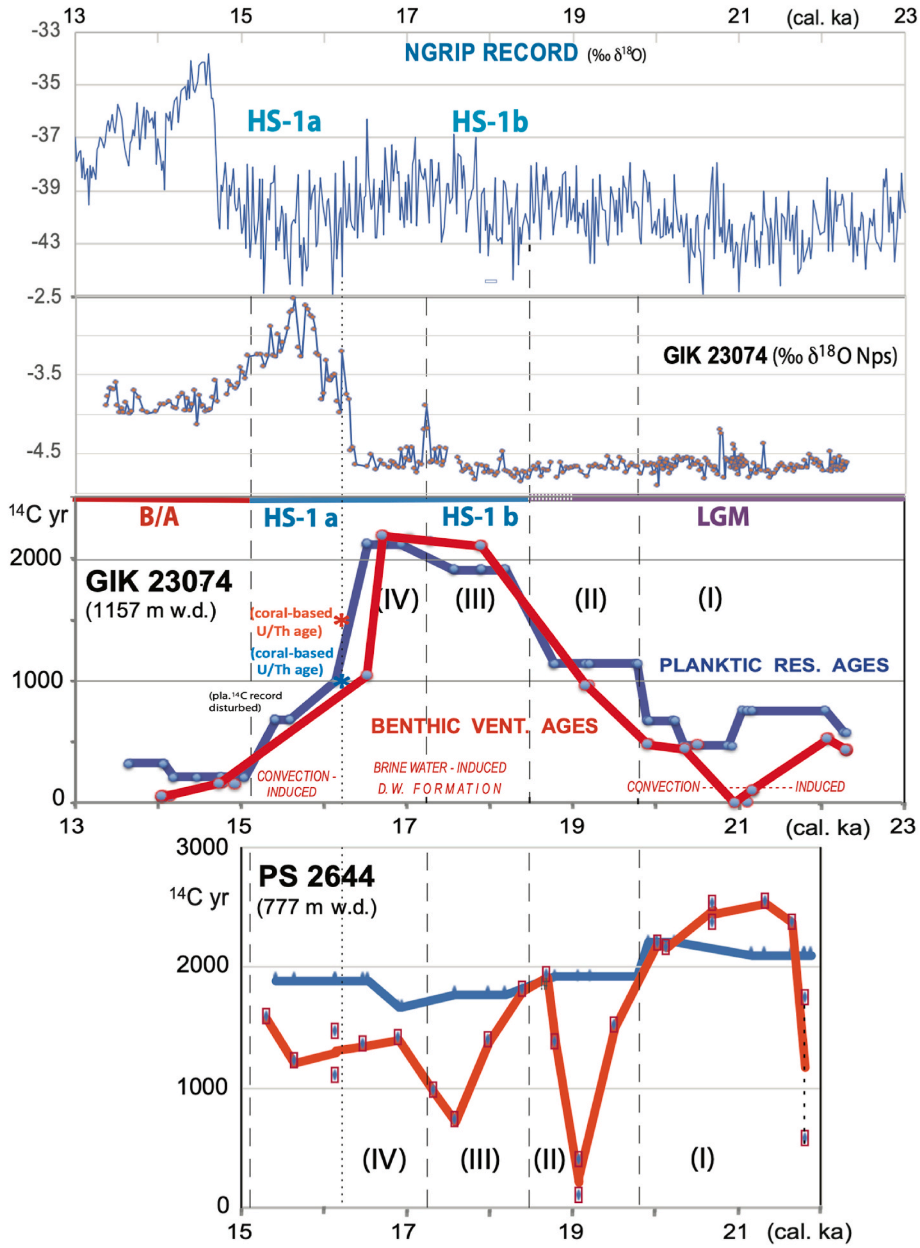

Fig. 3. Top panel: NGRIP $\delta^{18}O$ record vs. cal. ka b2k (GICC05, Wolff et al., 2010) as reference to centennial-scale climate changes in the northern hemisphere. Second panel: Prominent late-HS-1 minimum in planktic $\delta^{18}O$ record of Core GIK23074 records meltwater breakout from Barents Shelf ice, also reflected by a distinct cooling of HS-1a (topmost panel). Third panel: Planktic reservoir ages ("MRAs"; blue) and benthic ventilation age records (red) of sediment core GIK23074 document peak glacial-to-deglacial changes in surface and bottom water oceanography in the Norwegian Sea 23–13 cal. ka (before 1950 AD). Benthic ^{14}C ages are based on specimens of *Cribrononion teretis*. Blue and red asterisks mark two cal. age estimates of planktic and benthic foraminifera based on paired U/Th ages of a solitary coral (Dreger, 1999; plus unpubl. written comm. 2000). Lowermost panel: Planktic reservoir ages ("MRAs"; blue) and benthic ventilation age records (red) of sediment core PD2644 document peak glacial-to-deglacial changes in surface and bottom water oceanography in the Icelandic Sea 22–15 cal. ka (before 1950 AD). Benthic ^{14}C ages are based on specimens of epibenthic *Cibicidoides lobatulus*. — Roman numbers show time slices I to IV. Note, age scales of GIK 23074 and PS2644 records have not been aligned to the age scale of NGRIP but are independently based on atmospheric ^{14}C plateau tuning. (For interpretation of the references to color in this figure legend, the reader is referred to the Web version of this article.)

epibenthic $\delta^{13}C$ values (0.6–1.4 ‰) and just medium high benthic ventilation ages. They record reduced source water ventilation, thus trace a modest flux of dissolved organic carbon. At Site PS2644 DSO mode 3 started with an abrupt drop in maximum benthic $\delta^{18}O$ values of single epibenthic specimens by 0.8 ‰, that reflects a 3.4 °C rise in minimum bottom water temperature over less than 500 yr, shortly after a last high in bottom water ventilation age (Fig. 4). The $\delta^{18}O$ shift, however, was hardly linked to a brine-water related signal of freshwater dilution (Sessford et al., 2019), since paired local benthic ventilation ages of 700–1400 yr conflict with high MRA of 1800–2300 yr marking surface waters all over the Nordic Seas during early HS-1 (Figs. 2 and 3). The high MRA values were analyzed on Nps reflecting water depths of 50–200 m (Simstich et al., 2003). Here, $\delta^{18}O$ anomalies of Nps of HS-1 do not reveal any major pack ice-free anomalies as source of brine waters in the Nordic Seas *prior to* 16.3 cal. ka (Fig. 2b; Sarnthein et al., 2001: Fig. 12c).

Changes in minimum bottom water temperature at Site PS2644 compare well with Mg/Ca-based temperature changes reported for stadial and interstadial periods over MIS3 by Sessford et al. (2018) for twin sediment Core GS15-198-36CC. Here, minimum values of 1° to −1.5 °C

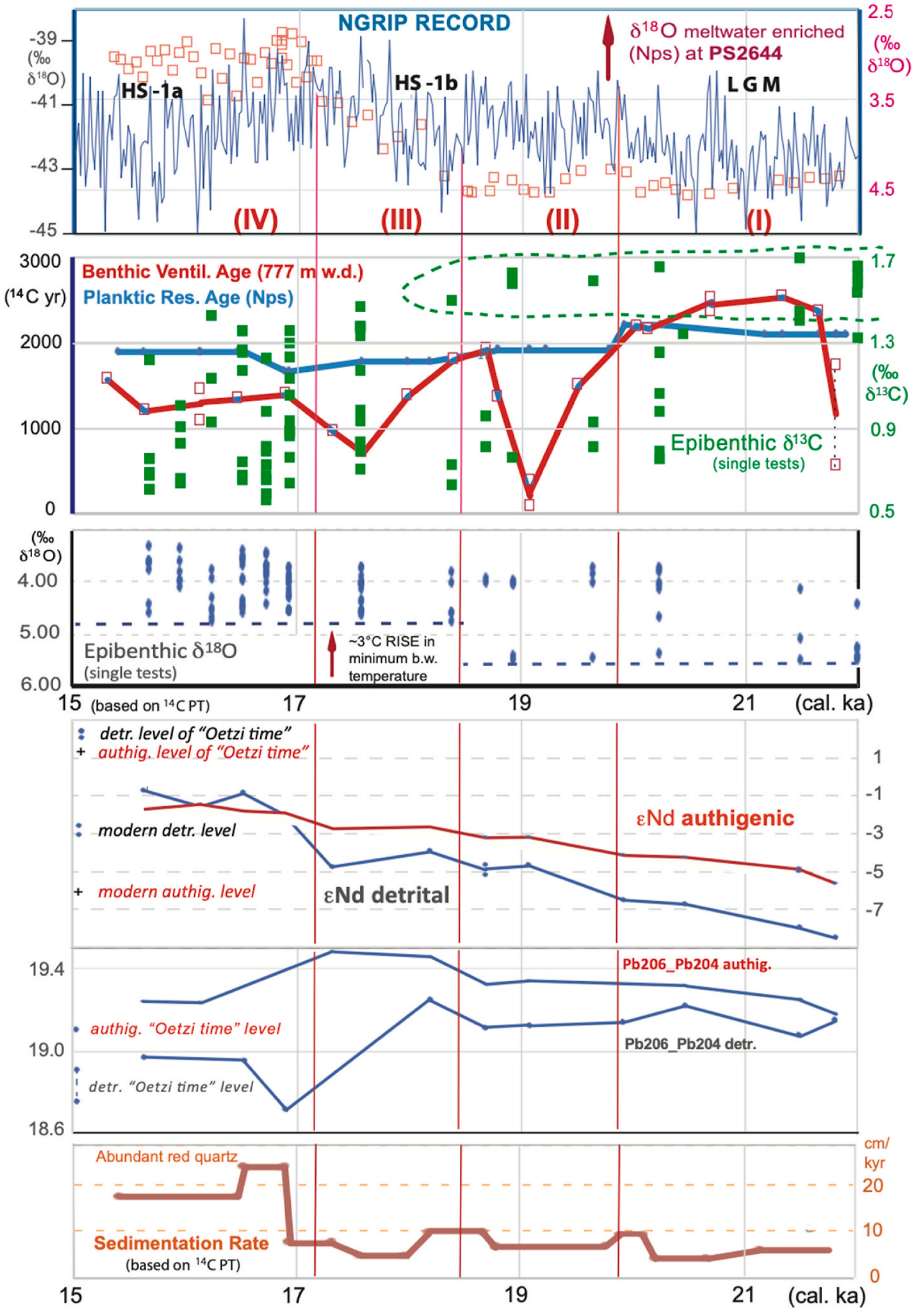

Fig. 4. Comparison of various proxy records from sediment core PS2644 that document peak glacial-to-deglacial changes in surface and bottom water oceanography at the northern entrance of the Denmark Strait 22–15 cal. ka (before 1950 AD). Age control based on ^{14}C plateau tuning technique. Top panel shows NGRIP $\delta^{18}O$ record of Greenland vs. cal. ka b2k (GICC05; Wolff et al., 2010) as reference to coeval changes in northern hemisphere climate plotted vs. planktic $\delta^{18}O$ record of SST rise and meltwater dilution of NIIC waters (Voelker, 1999). Roman numbers indicate time slices I to IV. Panel 2 shows planktic reservoir ages (i.e., MRA; red broken line), prominent changes in benthic ventilation age (blue line; Sarnthein et al., 2020), and two separate populations of epibenthic $\delta^{13}C$ values obtained from single foraminifera tests (Voelker, 1999). Panel 3 depicts epibenthic $\delta^{18}O$ values of single foraminifera tests (Voelker, 1999), where a 0.8 shift in maximum $\delta^{18}O$ reflects an abrupt 3.4 °C rise in minimum bottom water temperature near 18.4 cal. ka. Panel 4 shows gradual rise in the radiogenic ε_{Nd} portion of Nd isotopes of authigenic and detrital sediment fractions as compared to modern and mid-Holocene ("Oetzi time" ~5.7 cal. ka) values (Kutschera and Müller, 2003). Panel 5 shows variations in authigenic and detrital Pb206/Pb204 ratios. Panel 6 gives changes in bulk sedimentation rate (cm/kyr) as derived from cal. ages obtained by means of the ^{14}C plateau tuning technique (Sarnthein et al., 2020). (For interpretation of the references to color in this figure legend, the reader is referred to the Web version of this article.)

mark GI 5, 6, 7, and GI 8, when convection formed bottom waters nearby in the Nordic Seas. In turn, warm temperatures of 2°–4°/5 °C marked Greenland Stadials (GS) 4, 5, 7, 8, and the very onset of GI 8. The temperature anomalies reached up to 6 °C, hence provide crucial evidence for multiple substantial short-term changes in the origin and circulation geometry of DSO waters.

Circulation changes between time slices IIIand IV are further supported by a significant rise in εNd and drop in $^{206}Pb/^{204}Pb$ isotope ratios (Figs. 4 and 5). These proxies form important tracers of basaltic sediments from Iceland and/or the Iceland-Scotland Ridge, predominantly passed by mode-3 waters prior to reaching Site PS2644 (~68°N), such as the modern track of the North Iceland Jet (NIJ) today supplying almost half of the total DSO flow rate (Våge et al., 2011) (Figs. 1, 5 and 6). Less likely, the isotope ratios may trace an input from East Greenland

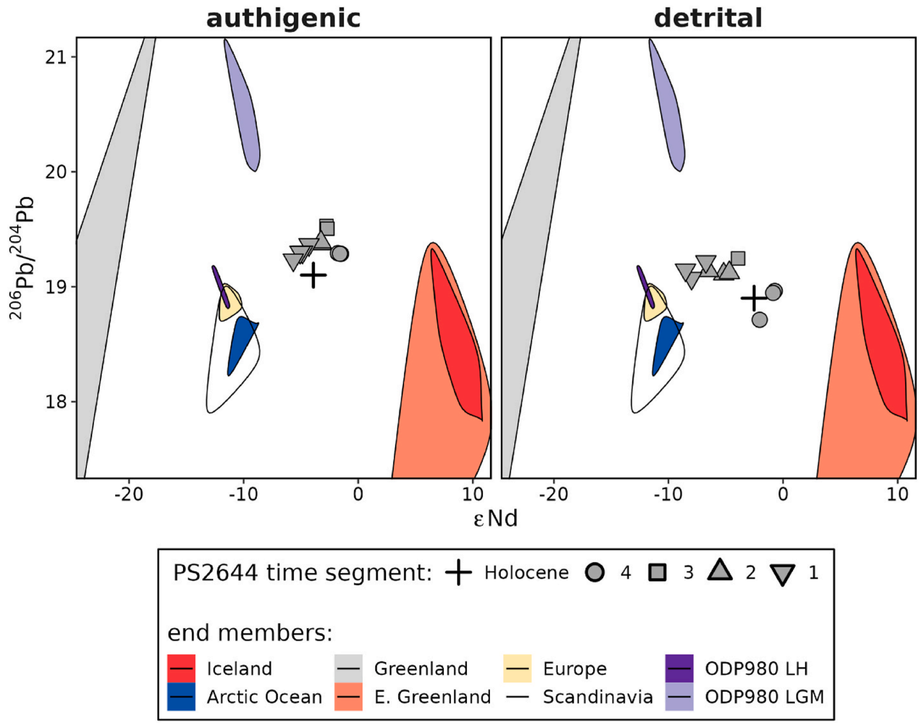

Fig. 5. Authigenic and detrital $^{206}Pb/^{204}Pb$ ratios vs. eNd at Site PS2644 and potential sediment sources (Table 3). PS2644 data are symbols indicating different time slices as described in the text. The Holocene sample was derived from a combination of eNd data at the core top and Pb isotope data from an ash layer at 18 cm depth, since the core top appeared to be contaminated by strongly unradiogenic anthropogenic lead. Potential end members are indicated as shaded areas (Crocker et al., 2016; Crocket et al., 2013; Eisenhauer et al., 1999; Fagel et al., 2002; Farmer et al., 2003; Haley et al., 2008; Kempton et al., 2000; Peate and Stecher, 2003; Struve et al., 2019). Data from ODP Site 980 in the Northeast Atlantic are from authigenic sediment fractions only. Greenland isotopic ratios span large ranges outside the limits of Fig. 5.

basalts (S of 70°N) (Peate and Stecher, 2003), since the EGC acts as interjacent barrier (Fig. 1).

After 18.4 cal. ka, the NIJ was established as dominant source of DSO mode-3 water. Besides by radiogenic-isotope records that suggest an enhanced input of basalt sediment (Fig. 5) as characteristic of the nearby Iceland-Scotland Ridge east of Iceland, this change in flow geometry is supported by some independent lines of proxy-based evidence showing a close link between waters at Site PS2644 and topmost Atlantic intermediate waters south and southeast of Iceland over HS-1: (i) Dominant epibenthic $\delta^{13}C$ values of 0.6–0.9 ‰ closely resemble 0.4–0.8 ‰ $\delta^{13}C$ at Site GIK23519 monitoring the output of DSO waters south of the Denmark Strait (Millo et al., 2006; Hagen and Hald, 2002; Sarnthein et al., 1994). (ii) The ventilation ages of DSO mode 3 (Fig. 4) match closely the ages of intermediate and subsurface waters recorded south of Iceland (Thornalley et al., 2011). (iii) Minimum temperatures of Atlantic Intermediate Waters (~4°C; Van Kreveld et al., 2000) that have fed the NIJ before crossing the Iceland-Scotland Ridge at depths of <200 m w.d. compare well with the minimum temperatures documented for bottom waters at Site PS2644 (Fig. 4).

By contrast to mode 2 the flow strength of DSO mode 3 decreased significantly or even became negligible over time slice IV, when bulk hemipelagic sedimentation rates at Site PS2644 increased suddenly from 5 to 10 up to >20 cm/ky (Fig. 4). The high rates were linked to abundant ice-rafted debris (IRD) rich in hematite-stained red quartz grains. They depict a discharge of Devonian 'Old Red' sediments picked up by icebergs along the N.E. Greenland margin (N of 72°30′N), thus reflect an ongoing afflux of EGC (Voelker, 1999).

On a centennial timescale, a fast rise of minimum bottom water temperatures by > 3 °C marked the onset of deglacial DSO mode 3, directly paired with the onset of major but gradual depletion of planktic $\delta^{18}O$ by up to 1.5 ‰ at PS2644 (Fig. 4). This drop reflects the arrival of both warmer and less saline surface waters advected from southwest through the Denmark Strait, a current analogous to the modern North Iceland branch of the Irminger Current (Sarnthein et al., 2001) (Fig. 1). Especially, however, the drop of planktic $\delta^{18}O$ was linked to a reduction of salinity induced by meltwaters possibly sourced in the ice sheet of West Greenland. Necessarily the reduction led to enhanced sea ice cover (Sadatzki et al., 2020; You et al., 2023). Only after 17.2 cal. ka, the onset of time slice IV, when meltwater advection had reached a stable maximum, census counts of planktic foraminifera started to display an SST rise by 2°–4 °C then contributing to $\delta^{18}O$ depletion (Voelker, 1999; Hagen and Hald, 2002).

Both the inflow of meltwaters and DSO mode 3 started right at 18.4 cal. ka, the base of deglacial time slice III. This event is precisely coeval with a major abrupt atmospheric cooling reflected by a decrease in $\delta^{18}O$ records of Greenland ice cores GRIP2 and NGRIP, thus has been used to define the onset of HS-1b (Table 2).

4.2. Changes of surface and deep-water circulation in the eastern Nordic Seas

In the eastern Nordic Seas planktic $\delta^{18}O$ values of 4.6–4.8 ‰ at Site GIK23074 did not show any substantial meltwater signal over the LGM and most of HS-1, from 22.3 to 16.3 cal. ka, except for a minor $\delta^{18}O$ low ~17.6–17.2 cal. ka (by $\Delta\delta^{18}O = -0.3$ ‰). Later, planktic $\delta^{18}O$ values display a major and almost abrupt drop by −2 ‰ at 16.3–16.0 cal. ka (Fig. 2b and 3). It clearly documents a major ice and meltwater outbreak nearby in the Nordic Seas, that started from the Barents shelf, spread south to Faeroe (Weinelt et al., 1991; Sarnthein et al., 2001), and led to a turbulent mixing of surface waters, at least down to water depths of 1157 m over >1000 yr until ~14.7 cal. ka (Fig. 3).

The meltwater signal started coeval with a $\delta^{18}O$ depletion and abrupt cooling recorded in ice cores GISP2 and NGRIP (Grootes and Stuiver, 1997) (Fig. 2b). Thus, we use this event to define the onset of HS-1a, per

Table 3a
Radiogenic Nd and Pb isotope data of authigenic sediment fractions in Core PS2644. Double standard deviation uncertainties are indicated with "u".

Sample depth (cm)	*Cal. age (ka)/PT to Suigetsu atm ^{14}C record*	Interval name/ time slice	Comment	eNd	u (eNd)	$^{206}Pb/^{204}Pb$	u ($^{206}Pb/^{204}Pb$)	$^{207}Pb/^{204}Pb$	u ($^{207}Pb/^{204}Pb$)	$^{208}Pb/^{204}Pb$	u ($^{208}Pb/^{204}Pb$)	$^{208}Pb/^{206}Pb$	u ($^{208}Pb/^{206}Pb$)	$^{207}Pb/^{206}Pb$	u ($^{207}Pb/^{206}Pb$)	$^{208}Pb/^{207}Pb$	u ($^{208}Pb/^{207}Pb$)
0	zero	Holocene, modern	anthrop. Pb contam.	−3.92	0.30	18.38470	0.00026	15.60775	0.00024	38.30583	0.00175	2.08360	0.00009	0.84896	0.00001	2.45433	0.00010
18		mid Holocene	ash layer	1.25	0.30	19.10072	0.00046	15.63563	0.00038	38.96135	0.00155	2.03979	0.00008	0.81859	0.00001	2.49184	0.00010
63.5	15.55	HS-1a/4		−1.78	0.30	19.29192	0.00434	15.66197	0.00159	39.10023	0.00371	2.02675	0.00018	0.81184	0.00006	2.49650	0.00009
74.5	16.17	HS-1a/4		−1.50	0.30	19.28612	0.00434	15.66204	0.00159	39.09438	0.00371	2.02707	0.00018	0.81208	0.00006	2.49615	0.00009
74.5	16.17	HS-1a/4		−1.60	0.30	19.28705	0.00434	15.66065	0.00159	39.09143	0.00371	2.02683	0.00018	0.81197	0.00006	2.49618	0.00009
81	16.53	HS-1a/4		−1.85	0.13												
88	16.88	HS-1a/4		−1.95	0.13												
94.5	17.39	HS-1b/3		−2.78	0.30	19.52870	0.00434	15.69832	0.00159	39.20421	0.00371	2.00753	0.00018	0.80386	0.00006	2.49736	0.00009
99.5	18.24	HS-1b/3		−2.70	0.30	19.50477	0.00434	15.69589	0.00159	39.19668	0.00376	2.00963	0.00018	0.80474	0.00006	2.49725	0.00009
104.5	18.74	LLGM/2		−3.25	0.30	19.37278	0.00434	15.67760	0.00159	39.13007	0.00371	2.01980	0.00018	0.80924	0.00006	2.49591	0.00009
107.5	19.15	LLGM/2		−3.25	0.30	19.38892	0.00434	15.68262	0.00159	39.14168	0.00371	2.01876	0.00018	0.80885	0.00006	2.49582	0.00009
113	19.92	LLGM/2		−4.18	0.13												
117	20.47	LGM/1		−4.29	0.30	19.36649	0.00434	15.68008	0.00159	39.11794	0.00371	2.01989	0.00018	0.80964	0.00006	2.49479	0.00009
121.5	21.57	LGM/1		−4.86	0.30	19.30191	0.00434	15.67095	0.00159	39.06195	0.00371	2.02373	0.00018	0.81189	0.00006	2.49260	0.00009
121.5	21.57	LGM/1		−5.07	0.30	19.30059	0.00434	15.67109	0.00159	39.06014	0.00371	2.02380	0.00018	0.81196	0.00006	2.49251	0.00009
123.5	21.89	LGM/1		−5.66	0.30	19.23342	0.00434	15.66390	0.00159	39.00911	0.00371	2.02819	0.00018	0.81441	0.00006	2.49037	0.00009

analogy to that of HS-1b being tied to an early deglacial meltwater incursion in the western Nordic Sea (Fig. 3).

Over time slices I and II, eastern surface waters show low MRA of ~500–800 and 1200 yr (Fig. 2b and 3). They closely resemble MRA values reported for very early LGM times (Simon et al., 2023), but strongly differ from the high MRA of 1900–2200 yr recorded at Site PS2644 in the west. After 18.4 cal. ka, contemporaneous with the start of meltwater incursion through the Denmark Strait, MRA at eastern Site 23074 depict a fast rise up to 1730–2000 yr, hence reach rapidly a close match with MRA found in the west over time slices II–IV (Figs. 2 and 3). Thus, the differential geometry of eastern and western surface water circulation of time slices I and II was terminated and briefly replaced by a close match over time slices III to lower IV. At that time, 'old' surface waters started to cover the complete eastern Nordic Seas, here suggesting an Arctic origin like those of the EGC. This flow scheme dominated until ~16.2 cal. ka, the onset of HS-1a (Fig. 3).

During the LGM, low bottom water ventilation ages at Site GIK 23074 indicate lively intermediate-water convection closely nearby in the eastern Nordic Sea, at least reaching down to ~1200 m w.d. (Figs. 3 and 6; in harmony with Meland et al., 2008; Thornalley et al., 2011). By contrast, waters at Site PS2644 continued to be stratified. Extremely young intermediate waters rarely found their way from eastern Site GIK23074 up to western Site PS2644, such as during time slice II (DSO mode 1; Fig. 4), when deep-water formation continued in the east, though somewhat attenuated (Fig. 3).

Based on a fast rise in MRA the circulation geometry of the eastern Nordic Seas was strongly modified after 18.4 cal. ka, when the inflow of warm and highly saline NAC was replaced by less saline surface waters that probably originated from the Arctic (Fig. 6). This change is reflected by a rise of local bottom water ventilation ages from <1000 yr up to 2100–2200 yr (Fig. 3). Thus, local intermediate and deep-water convection (*sensu* Siedler et al., 2001) were replaced by stable stratification. It lasted until 16.3 cal. ka, when the outlined great iceberg and meltwater outbreak from the Barents Sea immediately resulted in local stirring and overturning in the eastern Nordic Seas, that is, to renewed rejuvenation and ventilation of local intermediate waters (Fig. 3).

In addition, seasonal brine water formation has led to probably modest volumes of deep-water formation (Bauch and Bauch, 2001; Waelbroeck et al., 2011; Thornalley et al., 2011). During HS-1 time slices III – IV, however, brine water-induced intermediate waters have never spread from the eastern Nordic Seas up to the westernmost Nordic Seas to form DSO waters at Site PS2644, different from a model proposed by et al. (2019). Instead, waters at this site have been dominated by the North Iceland Jet (*sensu* Våge et al., 2011) that supplies waters from the northern slope of Iceland and ultimately, from upper North Atlantic Intermediate Waters, as outlined above.

4.3. Differential DSO modes and Nordic Sea stratification – implications for short-term glacial-to-deglacial climate change in the northern hemisphere

Near ~18.4 cal. ka, our benthic ventilation ages and ocean proxy data suggest a basic change of circulation geometry both in the western and eastern Nordic Seas, that subsequently differed strongly from today: Instead of Nordic Sea intermediate waters the NIJ started to feed the DSO northwest of Iceland, at Site PS2644, below a flow of highly aged, less saline EGC surface waters advected from the Arctic (Fig. 2a, 4 and 6). Within the error range of ^{14}C plateau tuning technique (Sarnthein et al., 2020, Table 2) the switch occurred almost instantaneous between 18.7 and 18.4 cal. ka and was aligned with (i) a very first incursion of deglacial meltwaters through the Denmark Strait and (ii) a switch from anti-estuarine to estuarine geometry of surface and intermediate-water circulation of the Norwegian Sea (Figs. 4 and 6).

The switch also presents a tipping point of circulation geometry in the North Atlantic (AMOC), as depicted by a coeval major abrupt rise in MRA near to the Azores Islands (Balmer and Sarnthein, 2018). In turn,

Table 3b
Radiogenic Nd and Pb isotope data of detrital sediment fractions in Core PS2644. Double standard deviation uncertainties are indicated with "u".

sample depth (cm)	*cal. age (ka)/PT to Suigetsu atm ^{14}C record*	interval name/ time slice	comment	εNd	u (εNd)	$^{206}Pb/^{204}Pb$	u ($^{206}Pb/^{204}Pb$)	$^{207}Pb/^{204}Pb$	u ($^{207}Pb/^{204}Pb$)	$^{208}Pb/^{204}Pb$	u ($^{208}Pb/^{204}Pb$)	$^{208}Pb/^{206}Pb$	u ($^{208}Pb/^{206}Pb$)	$^{207}Pb/^{206}Pb$	u ($^{207}Pb/^{206}Pb$)	$^{208}Pb/^{207}Pb$	u ($^{208}Pb/^{207}Pb$)
0	zero	Holocene, modern	anthrop. Pb contam.	−2.53	0.3	18.49703	0.00050	15.5873	0.00043	38.50056	0.00184	2.08173	0.00011	0.84261	0.00001	2.47045	0.00014
0	zero	Holocene, modern	anthrop. Pb contam.	−3.04	0.3												
18		mid Holocene	ash layer	2.41	0.3	18.74050	0.00165	15.45869	0.00144	38.37519	0.00501	2.04778	0.00019	0.82464	0.00002	2.48302	0.00027
18		mid Holocene	ash layer	2.45	0.3												
18		mid Holocene		2.05	0.3	18.90047	0.00060	15.58000	0.00052	38.70315	0.00253	2.04782	0.00013	0.82432	0.00001	2.48425	0.00016
63	15.55	HS-1a/4		−0.72	0.3	18.96305	0.00038	15.60107	0.00029	38.77364	0.00170	2.04488	0.00011	0.82259	0.00001	2.48576	0.00013
74	16.17	HS-1a/4		−1.55	0.3												
81	16.53	HS-1a/4		−0.87	0.3	18.94612	0.00035	15.59702	0.00037	38.90443	0.00122	2.05344	0.00006	0.82322	0.00001	2.49442	0.00009
88	16.88	HS-1a/4		−2.04	0.3	18.71245	0.00033	15.58099	0.00027	38.48618	0.00195	2.05678	0.00009	0.83265	0.00001	2.47014	0.00011
94	17.39	HS-1b/3		−4.8	0.3												
99	18.24	HS-1b/3		−3.93	0.3	19.24595	0.00041	15.65537	0.00039	39.09665	0.00168	2.03142	0.00008	0.81344	0.00001	2.49734	0.00010
104	18.74	LLGM/2		−5.18	0.3	19.10960	0.00033	15.63546	0.00030	38.85739	0.00148	2.03340	0.00009	0.81820	0.00001	2.48522	0.00011
104	19.15	LLGM/2		−4.69	0.3												
107	19.92	LLGM/2		−4.69	0.3	19.12211	0.00032	15.64079	0.00029	38.97333	0.00245	2.03815	0.00013	0.81795	0.00001	2.49180	0.00016
113	20.47	LGM/1		−6.51	0.3	19.13902	0.00045	15.64649	0.00037	38.90014	0.00207	2.03254	0.00012	0.81752	0.00001	2.48624	0.00015
116.5	21.57	LGM/1		−6.74	0.3	19.21819	0.00045	15.65468	0.00038	38.93230	0.00173	2.02585	0.00010	0.81458	0.00001	2.48701	0.00012
121	21.57	LGM/1		−7.98	0.3	19.07373	0.00042	15.63338	0.00038	38.94588	0.00152	2.04186	0.00010	0.81963	0.00001	2.49119	0.00011
123	21.89	LGM/1		−8.51	0.3	19.14619	0.00039	15.64844	0.00044	38.91836	0.00102	2.03272	0.00008	0.81732	0.00001	2.48710	0.00011

the switch led to a prompt breakdown of the poleward advection of warm Atlantic surface waters and heat that drove the "Nordic Heat Pump" up to northern Norway and Svalbard during the LGM. Yet, the peak-glacial heat flow had been somewhat reduced compared to today (SST records based on % Nps and Artificial Neural Network estimates of foraminifera species counts; Weinelt et al., 2003).

Accordingly, the salient tipping point of northern hemisphere climate is also monitored in the $\delta^{18}O$ record of NGRIP (GICC05; Wolff et al., 2010). From 22 to ~17 cal. ka, temperatures in North Greenland reflect an overall trend of gradual deglacial warming (Figs. 2 and 3). This long-term trend, however, was interrupted by a first significant breakdown in the deglacial advection of warm atmospheric moisture, an event that started between 18,500 and 18,380 cal yr b2k, here named onset of 'HS-1b'. The switch was less distinct in ice core GISP2, here depicted between 18,630 and 18,430 cal yr b2k (Grootes and Stuiver, 1997), an age range that matches the great switch in seawater stratification of Nordic Sea circulation within the range of a century (Table 2).

Per se, the close match of ages derived from ice core records and from plateau tuning of ocean ^{14}C ages serves as beautiful evidence for the robustness of age estimates based on the ^{14}C-plateau tuning technique. Also, the switch of Atlantic circulation geometry is reflected directly by a special short atmospheric ^{14}C plateau between ~18.6 and ~18.4 cal. ka before 1950 AD, named Plateau '4a' (Fig. 2a and b; Sarnthein et al., 2023). Based on GICC05 ages, the fundamental switch in seawater stratification and the resulting drop of the Nordic heat pump probably took no longer than 80–100 yr.

Unfortunately, it is widely impossible to compare this narrow age range with any of the numerous IRD and SST records published for the onset of HS-1 from the North Atlantic "Heinrich-1 IRD Belt". Except for some sporadic and wide-spaced single age tie points (Hodell et al., 2017; and refs. therein), local MRA levels and even more so, the precise timing of their short-term variations are largely unknown due to a lack of sediment records with pertinent cal. age values such as those generated by high-resolution ^{14}C plateau tuning. By comparison to the changes recovered in the Nordic Seas over HS-1 (Fig. 2a and b) local MRAs may actually have been subject to short-term variations by 200–2000 yr. Also, the age range of meltwater advection and ice-rafted debris input was subject to major regional variations, while winds and currents were driving icebergs over vast sea regions.

Off southwestern Portugal, for example, ^{14}C ages of sediment record SHAK06-5K were calibrated by ^{14}C plateau tuning (Ausin et al., 2021) and show a $\delta^{18}O$-based local meltwater incursion and IRD input not starting prior to 17.8/17.9 cal. ka, that is 500–600 yr after the start of HS-1b, as defined in Nordic Seas cores. In turn, the HS-1 cold spell is also reported for the ^{10}Be-dated 'Gschnitz Stadial' of the Alpine Late Glacial. The maximum of this glacial advance reflects temperatures and aridity values close to those estimated for the LGM and is constrained at 16.8 ± 1.7 cal. ka (Ivy-Ochs, 2015).

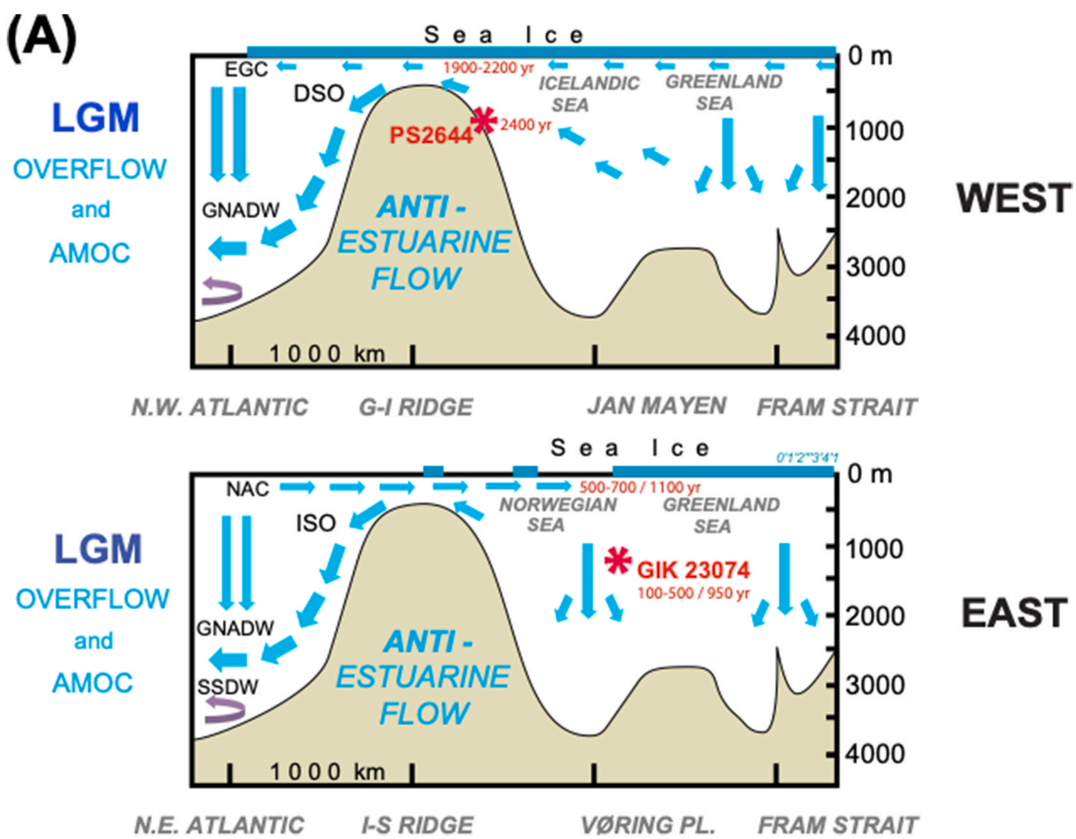

Fig. 6. Vertical transects of hypothetical circulation geometry across the western and eastern Nordic Seas between North Atlantic, Greenland-Island (GI)/Island-Scotland (I–S) Ridge, and Fram Strait (schemes modified from Thornalley et al., 2011), showing deep- and intermediate-water convection separately for the eastern (lower panel) and western (upper panel) Nordic Seas. Grey arrow colors indicate brine water-induced intermediate waters and weak anti-estuarine overflow. Transect (A) for LGM, transect (B) for HS-1 times starting at 18.4 cal. ka. Red asterisks: Core sites PS2644 and 23074. Red numbers give prime evidence, the range of local planktic reservoir ages (MRA) and benthic ventilation ages. Pertinent MRA and bottom water ventilation ages for core sites RAPID-10-1P and RAPID-17-5P south of the Iceland-Scotland Ridge are from Thornalley et al. (2011). SSDW = Southern Source Deep Water, GA SSW = Glacial Atlantic Southern Source Waters, NIJ = North Iceland Jet, DSO = Denmark Strait Overflow, ISO = Iceland Strait Overflow, EGC = East Greenland Current. Estimates of full and partial sea ice cover for LGM and Heinrich transects are based on Sadatzki et al., 2020, and Sessford et al. (2019). — Note, in our view, MRA values and benthic ventilation ages listed by Thornalley et al. (2011, 2015) and in part incorporated in Fig. 6B may not reflect true past values (1) because of a lack of precise atm. age calibration (leading to little evidenced MRAs), (2) since a majority of age samples were based on *Pyrgo*, etc. species that are strongly subject to the bias of "old" pore waters in the ambient sediment (Magana et al., 2010). (For interpretation of the references to color in this figure legend, the reader is referred to the Web version of this article.)

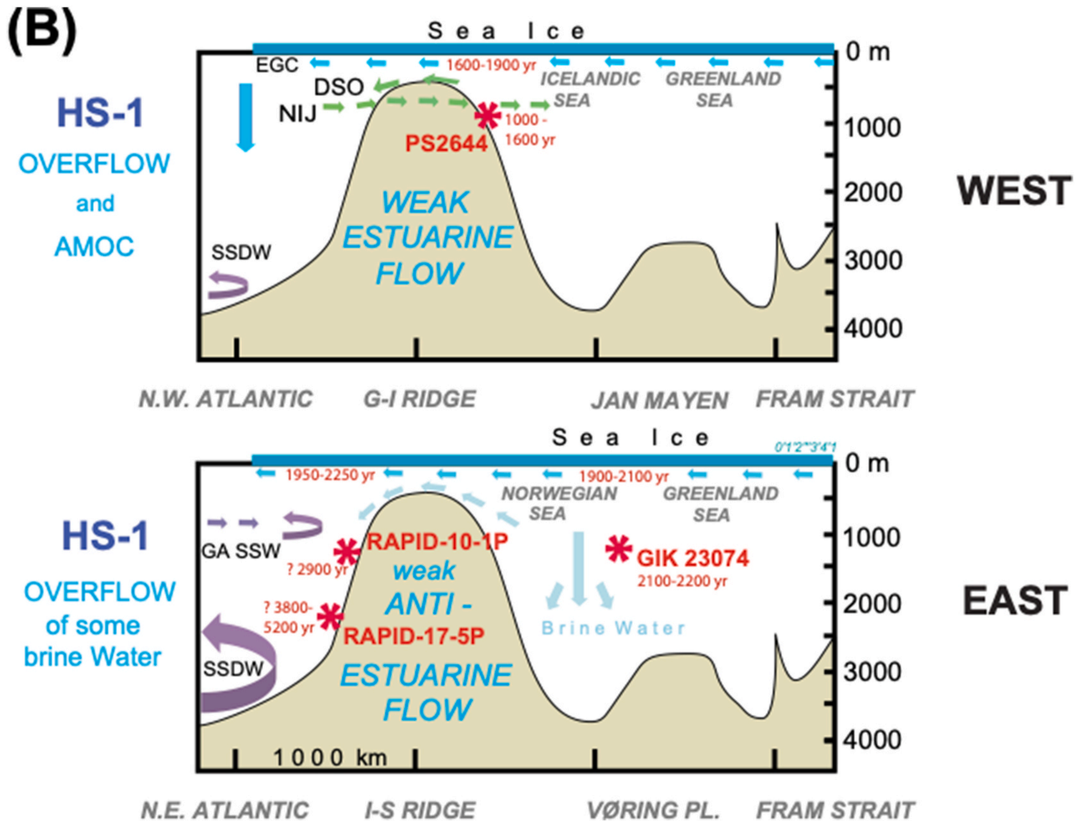

Fig. 6. (*continued*).

The mechanisms for the onset of cold spell HS-1b form a scenario enticing to speculate about trends of 'Global Warming' found today and possibly, in the near future (e.g., models of Ditlevsen and Ditlevsen, 2023; Jansen et al., 2020; Caesar et al., 2018). In summary, this view is based on various boundary conditions: (i) Within a century the onset of the cold spell near 18.4 cal. ka was coeval in two records from both Greenland ice cores and two marine sediment records. They showed a fundamental switch from anti-estuarine to modified anti-estuarine flow geometry in the western and eastern Nordic Seas, moreover, in AMOC. (ii) The tipping point of seawater stratification was met as soon as first meltwaters had passed the Denmark Strait. (iii) Overall, the switch in the Nordic Seas and sequentially, the breakdown of Nordic Heat Pump took <200 yr.

5. Conclusions

- The close match of cal. age estimates based on both ^{14}C-PT and the incremental age scale of Greenland ice cores supports the accuracy of the PT technique and brings new insights on deglacial changes in MRA: 'The proof of the pudding is in the eating'.
- Based on the ^{14}C PT we define for Sites PS2644 and GIK 23074 a suite of four peak glacial to early-deglacial time slices 22-15 cal. ka. They show differential MRAs and bottom water ventilation ages in the western and eastern Nordic Seas.
- Sediment-based quantitative proxy-data from the northern entrance to the Denmark Strait suggest the definition of three glacial-to-deglacial modes of the Denmark Strait Overflow (DSO) earmarked by diverse source regions and/or flow strength. DSO modes 1 and 2 largely carried a mix of intermediate and deep waters from the eastern Nordic Seas and Arctic and either reflect a weaker (DSO mode 2) or stronger or even erosive (DSO mode 1) anti-estuarine flow geometry, analogous to today.
- After 18.4 cal. ka, the proxy records of time slices III–IV suggest the abrupt onset of fundamentally different DSO mode 3. It was induced by an advection of meltwater-diluted surface waters from southwest though the Denmark Strait, a precursor of the modern Irminger Current. DSO mode 3 was fed by shallow subsurface waters of the North Iceland Jet (NIJ), >3 °C warmer than those of antecedent DSO mode 2. The NIJ supplied upper intermediate waters from the North Atlantic south and southeast of Iceland, hence suggests a strong weakening of local anti-estuarine flow geometry, coeval with the end of deep-water convection in the eastern Nordic Sea.
- The fast change in Nordic Seas flow geometry near ~18.4 cal. ka is paired with a special short atmospheric ^{14}C plateau 4a.
- The switch of DSO flow geometry near 18.4 cal. ka was linked to a temporary end of the poleward heat flow named 'Nordic Heat Pump' and an end of deepwater convection in the eastern Nordic Seas. This change was precisely coeval with a distinct drop of Greenland temperatures recorded in ice cores GISP2 and NGRIP. The switch thus formed a major climate tipping point that hardly took more than a century and served as marker to define the onset of Heinrich stadial 1b.
- After 16.3 cal. ka, a major ice meltwater outbreak from the Barents shelf (Weinelt et al., 1991) caused changes in the flow geometry of the eastern Nordic Seas and further cooling of HS-1, thenceforward named HS-1a. It lasted until Dansgaard-Oeschger Event 1, as independently depicted in Greenland ice cores (~16.1–14.7 cal. ka).

Data availability

Data of Tables 1 and 3, moreover, planktic and benthic stable isotope data of cores PS2644 and GIK23074, that are employed in this study, have been submitted for uploading to PANGAEA.de® (PDI-39859).

Authors contribution

M.S. designed the research project.

M.S. introduced the technique of ^{14}C plateau tuning to re-calibrate and supplement ^{14}C ages of (published) high-resolution proxy records from the Nordic Seas.

P.B. contributed new radiogenic isotope data.

Both M.S. and P.B. closely cooperated on the details of the manuscript draft.

Declaration of competing interest

"Author A has not received any research funding. Author B obtained funding from the European Union's Horizon 2020 Research and 727 innovation program."

Acknowledgments

We thank Pieter M. Grootes, Kiel, and Antje Voelker, Lisboa, for substantial critical comments on our manuscript and for references to recent publications. Particularly, we thank A. Biastoch, Kiel, for his advice in potential questions of physical oceanography, and Patrick Rafter, Irvine, as reviewer of the manuscript for his highly constructive comments. We gratefully acknowledge the help of Ralf Tiedemann, AWI Bremerhaven, with the acquisition of special additional sediment samples from Core PS2644, John Southon, Irvine CA, and Gesine Mollenhauer, AWI Bremerhaven, for analyzing ^{14}C ages of benthic foraminifera samples of Core GIK23074, and Michael Bollen for help with the analysis of Nd and Pb isotope data at the University of Lausanne. Sebastian Beil, Kiel, and Hugo Ortner, Innsbruck, kindly helped us with software problems. P.B. acknowledges funding from the European Union's Horizon Europe research and innovation program (grant agreements No 101065424, project OxyQuant).

Appendix A. Supplementary data

Supplementary data to this article can be found online at https://doi.org/10.1016/j.quascirev.2025.109181.

References

Andrews, J.T., Voelker, A.H.L., 2018. "Heinrich events" (& sediments): a history of terminology and recommendations for future usage. Quat. Sci. Rev. 187, 31–40.

Ausin, B., Sarnthein, M., Haghipour, N., 2021. Glacial-to-deglacial reservoir and ventilation ages on the southwest Iberian continental margin. Quat. Sci. Rev. 255 (1–12), 106818.

Balmer, S., Sarnthein, M., 2018. Glacial-to deglacial changes in North Atlantic meltwater advection and deep-water formation – centennial-to-millennial-scale ^{14}C records from the Azores Plateau. Geochem. Cosmochim. Acta 236, 399–415. https://doi.org/10.1016/j.gca.2018.03.001.

Bard, E., Heaton, T.J., 2021. On the tuning of plateaus in atmospheric and oceanic ^{14}C records to derive calendar chronologies of deep-sea cores and records of ^{14}C marine reservoir age changes. Clim. Past 17, 1701–1725. https://doi.org/10.5194/cp-17-1701-2021.

Bauch, D., Bauch, H., 2001. Last glacial benthic foraminiferal $\delta^{18}O$ anomalies in the polar North Atlantic: a modern analogue evaluation. J. Geophys. Res. 106 (C5), 9135–9143.

Biastoch, A., Kaese, R.H., Stammer, D.B., 2003. The sensitivity of the Greenland-Scotland Ridge Overflow to forcing changes. J. Phys. Oceanogr. 33, 2307–2319.

Biastoch, A., Schwarzkopf, F.U., Getzlaff, K., Rühs, S., Martin, T., Scheinert, M., Schulzki, T., Handmann, P., Hummels, R., Böning, W.C., 2021. Regional imprints of changes in the Atlantic Meridional Overturning Circulation in the eddy-rich ocean model VIKING20X. Ocean Sci. 17, 1177–1211.

Birks, H.H., Gulliksen, S., Haflidason, H., Mangerud, J., Possnert, G., 2017. New radiocarbon dates for the Vedde ash and Saksunavatn ash from Western Norway. Quat. Res. 45, 119–127.

Blaser, P., Gutjahr, M., Pöppelmeier, F., Frank, M., Kaboth-Bahr, S., Lippold, J., 2020. Labrador Sea bottom water provenance and REE exchange during the past 35,000 years. Earth Planet Sci. Lett. 542, 1–12, 116299.

Blaser, P., Lippold, J., Gutjahr, M., Frank, N., Link, J.M., Frank, M., 2016. Extracting foraminiferal seawater Nd isotope signatures from bulk deep-sea sediment by chemical leaching. Chem. Geol. 439, 189–204. https://doi.org/10.1016/j.chemgeo.2016.06.024.

Bollhöffer, A., Eisenhauer, A., Frank, N., Pech, D., Mangini, A., 1996. Thorium and uranium isotopes in a manganese nodule from the Peru basin determined by alpha spectrometry and thermal ionization mass spectrometry (TIMS): are manganese supply and growth related? Geol. Rundsch. 85, 577–585.

Brakstad, A., Gebbie, G., Våge, K., Jeansson, E., Olafsdottir, S.R., 2023. Formation and pathways of dense water in the Nordic Seas based on a regional inversion. Prog. Oceanogr. 212, 102–981. https://doi.org/10.21335/NMDC-1271328906.

Bronk Ramsey, C., Heaton, T.J., Schlolaut, G., Staff, R.A., Bryant, C.L., Lamb, H.F., Marshall, M.H., Nakagawa, T., 2020. Reanalysis of the atmospheric radiocarbon calibration record from Lake Suigetsu, Japan. Radiocarbon. https://doi.org/10.1017/RDC2020/18.

Caesar, L., Rahmstorf, S., Robinson, A., Feulner, G., Saba, V., 2018. Observed fingerprint of a weakening Atlantic Ocean overturning circulation. Nature 556, 191–196.

Crocker, A.J., Chalk, T.B., Bailey, I., Spencer, M.R., Gutjahr, M., Foster, G.L., Wilson, P.A., 2016. Geochemical response of the mid-depth Northeast Atlantic Ocean to freshwater input during Heinrich events 1 to 4. Quat. Sci. Rev. 151, 236–254. https://doi.org/10.1016/j.quascirev.2016.08.035.

Crocket, K.C., Vance, D., Foster, G.L., Richards, D.A., Tranter, M., 2013. Continental weathering fluxes during the last glacial/interglacial cycle: insights from the marine sedimentary Pb isotope record at Orphan Knoll, NW Atlantic. Quat. Sci. Rev. 38, 89–99. https://doi.org/10.1016/j.quascirev.2012.02.004.

Ditlevsen, P., Ditlevsen, S., 2023. Warning of forthcoming collapse of the Atlantic meridional overturning circulation. Nat. Commun. 14 article no. 4254.

Dreger, D., 1999. Decadal-to-centennial-scale Sediment Records of Ice Advance on the Barents Shelf and Meltwater Discharge into the North-Eastern Norwegian Sea over the Last 40 kyr, D.Sc. Thesis. Univ. of Kiel, Kiel, pp. 1–79.

Duplessy, J.-C., Labeyrie, L., Waelbroeck, C., 2002. Constraints on the ocean oxygen isotopic enrichment between the last glacial maximum and the Holocene: paleoceanographic implications. Quat. Sci. Rev. 21, 315–330.

Eisenhauer, A., Meyer, H., Rachold, V., Tutken, T., Wiegand, B., Hansen, B.T., Spielhagen, R.F., Lindemann, F., Kassens, H., 1999. Grain size separation and sediment mixing in Arctic Ocean sediments: evidence from the strontium isotope systematic. Chem. Geol. 158, 173–188. https://doi.org/10.1016/S0009-2541(99)00026-1.

Fagel, N., Innocent, C., Gariepy, C., Hillaire-Marcel, C., 2002. Sources of Labrador Sea sediments since the last glacial maximum inferred from Nd-Pb isotopes. Geochem. Cosmochim. Acta 66, 2569–2581.

Farmer, G.L., Barber, D., Andrews, J., 2003. Provenance of late quaternary ice-proximal sediments in the North Atlantic: Nd, Sr and Pb isotopic evidence. Earth Planet Sci. Lett. 209, 227–243. https://doi.org/10.1016/S0012-821X(03)00068-2.

Grootes, P.M., Stuiver, M., 1997. $^{18}O/^{16}O$ variability in snow and ice with 10^{-3} to 10^{-5} year time resolution. J. Geophys. Res. 102 (C12), 26,455-26,470.

Hagen, S., Hald, M., 2002. Variation in surface and deep-water circulation in the Denmark Strait, North Atlantic, during marine isotope stages 3 and 2. Paleoceanography 17 (4), 13–16, 13-1.

Haine, T.W.N., 2021. A conceptual model of polar overturning circulations. J. Phys. Oceanogr. 51, 727–744.

Haley, B.A., Frank, M., Spielhagen, R.F., Fietzke, J., 2008. Radiogenic isotope record of Arctic Ocean circulation and weathering inputs of the past 15 million years. Paleoceanography 23. https://doi.org/10.1029/2007PA001486.

Hanebuth, T.J.J., Stattegger, K., Bojanowski, A., 2009. Termination of the last glacial maximum sea-level low-stand: the sunda-shelf data revisited. Global Planet. Change 66, 76–84.

Hansen, B., Østerhus, S., 2000. North atlantic-nordic seas exchange. Prog. Oceanogr. 45, 109–208. https://doi.org/10.1016/S0079-6611(99)00052-X.

Hodell, D.A., Nicholl, J.A., Bontognali, T.R.R., 2017. Anatomy of Heinrich Layer 1 and its role in the last deglaciation. Paleoceanography 32, 284–303. https://doi.org/10.1002/2016PA00302 plus 9 coauthors.

Hubberten, H.-W., 1995. Die Expedition Arktis-X2 mit FS "Polarstern" in 1994. Ber. Polarforsch. 174, 186.

Ivy-Ochs, S., 2015. Glacier variations in the European Alps at the end of the last glaciation. Cuadernos de Investigación Geográfica 41, 295–315.

Jansen, E., Hesselberg Christensen, J., Dokken, T., et al., 2020. Past perspectives on the present era of abrupt Arctic climate change. Nat. Clim. Change 10, 714–721.

Kaese, R.H., Oschlies, A., 2000. Flow through Denmark strait. J. Geophys. Res. C Oceans Atmos. 105 (28), 527–528, 546.

Kaese, R.H., Girton, J.B., Sanford, T.B., 2003. Structure and variability of the Denmark Strait Overflow: model and observations. J. Geophysical Research, Oceans 108 (C6). https://doi.org/10.1029/2002JC001548.

Kempton, P.D., Fitton, J.G., Saunders, A.D., Nowell, G.M., Taylor, R.N., Hardarson, B.S., Pearson, G., 2000. The Iceland plume in space and time: a Sr–Nd–Pb–Hf study of the North Atlantic rifted margin. Earth Planet Sci. Lett. 177, 255–271. https://doi.org/10.1016/S0012-821X(00)00047-9.

Kösters, F., 2004. Denmark Strait overflow: comparing model results and hydraulic transport estimates. J. Geophys. Res. C Oceans Atmos. 109, C10011. https://doi.org/10.1029/2004JC002297.

Kösters, F., Kaese, R.H., Schmittner, A., Herrmann, P., 2005. The effect of Denmark Strait Overflow on the atlantic meridional overturning circulation. Geophys. Res. Lett. 32, L04602. https://doi.org/10.1029/2004GL022112.

Kuijpers, A., Troelstra, S.R., Prins, M.A., et al., 2003. Late Quaternary sedimentary processes and ocean circulation changes at the southeast Greenland margin. Mar. Geol. 195, 109–129.

Kutschera, W., Müller, W., 2003. "Isotope language" of the alpine iceman investigated with AMS and MS. Nucl. Instrum. Methods Phys. Res. B204, 705–719.

Larkin, C.S., Ezat, M.M., Spielhagen, R., Bauch, H., Noormets, R., Polyak, L., Moreton, S., Roberts, N.L., Rasmussen, T.L., Sarnthein, M., Tipper, E.T., Piotrowski, A.M., 2022.

Resolving Nordic Seas deep-water formation during the last glacial maximum. Nat. Geosci. 15, 1–7. https://doi.org/10.1038/s41561-022-01050-w.
Lomitschka, M., Mangini, A., 1999. Precise Th/U-dating of small and heavily coated samples of deep-sea corals. Earth Planet Sci. Lett. 170, 391–401.
Macrander, A., Käse, R.H., Send, U., Valdimarsson, H., Jónsson, S., 2007. Spatial and temporal structure of the Denmark Strait Overflow revealed by acoustic observations. Ocean Dynam. 57, 75–89.
Magana, A.L., Southon, J.R., Kennett, J.P., Brendan, Roark E., Sarnthein, M., Stott, L.D., 2010. Resolving the cause of large differences between deglacial benthic fauna radiocarbon measurements in the Santa Barbara Basin. Paleoceanography 25, PA4102. https://doi.org/10.1029/2010PA002011,2010.
Meland, M.Y., Dokken, T.M., Jansen, E., Hevrøy, K., 2008. Water mass properties and exchange between the Nordic seas and the northern North Atlantic during the period 23–6 ka: benthic oxygen isotopic evidence. Paleoceanography 23. https://doi.org/10.1029/2007PA001416.
Millo, C., Sarnthein, Ms, Erlenkeuser, H., 2006. Variability of the Denmark Strait Overflow during the last glacial maximum. Boreas 35, 50–60.
Mix, A.C., Bard, E., Schneider, R., 2001. Environmental processes of the Ice age: land, oceans, glaciers (EPILOG). Quat. Sci. Rev. 20, 627–658.
Neff, U., Bollhoffer, A., Frank, A., Mangini, A., 1999. Explaining discrepant depth profiles of 234U/238U and 230Th$_{exec}$ in Mn-crusts. Geochem. Cosmochim. Acta 63 (15), 2211–2218. https://doi.org/10.1016/S0016-7037(99)00135-0.
Peate, D.W., Stecher, O., 2003. Pb isotope evidence for contributions from different Iceland mantle components to Palaeogene East Greenland flood basalts. Lithos 67, 39–52. https://doi.org/10.1016/S0024-4937(02)00250-5.
Pflaumann, U., Sarnthein, M., Chapman, M., d'Abreu, L., 2003. Glacial North Atlantic: sea-surface conditions reconstructed by GLAMAP 2000. Paleoceanography 18 (3), 1065. https://doi.org/10.1029/2002PA000774 plus 10 coauthors.
Sadatzki, H., Maffezzoli, N., Dokken, T.M., 2020. Rapid reductions and millennial-scale variability in Nordic Seas' sea ice cover during abrupt glacial climate changes. Proc. Natl. Acad. Sci. USA 117 (47), 29478–29486 plus 9 coauthors.
Sarnthein, M., Winn, K., Jung, S.J., Duplessy, J.C., Labeyrie, L., Erlenkeuser, H., Ganssen, G., 1994. Changes in east Atlantic deep-water circulation over the last 30,000 years: eight time slice reconstructions. Paleoceanography 9 (2), 209–267.
Sarnthein, M., Stattegger, K., Dreger, D., Erlenkeuser, H., Grootes, P., Haupt, B., Jung, S., Kiefer, T., Kuhnt, W., Pflaumann, U., Schäfer-Neth, C., Schulz, H., Schulz, M., Seidov, D., Simstich, J., van Kreveld-Alfane, S., Vogelsang, E., Völker, A., Weinelt, M., 2001. Fundamental modes and abrupt changes in North Atlantic circulation and climate over the last 60 ky - concepts, reconstruction, and numerical modelling. In: Schäfer, P., et al. (Eds.), The Northern North Atlantic: A Changing Environment. Springer Verlag, pp. 365–410.
Sarnthein, M., Balmer, S., Grootes, P.M., Mudelsee, M., 2015. Planktic and benthic ^{14}C reservoir ages for three ocean basins, calibrated by a suite of ^{14}C plateaus in the glacial-to-deglacial Suigetsu atmospheric ^{14}C record. Radiocarbon 57, 129–151.
Sarnthein, M., Küssner, K., Grootes, P.M., Ausin, B., Eglinton, T., Muglia, J., Muscheler, R., Schlolaut, G., 2020. Plateaus and jumps in the atmospheric radiocarbon record – potential origin and value as global age markers for glacial-to-deglacial paleoceanography, a synthesis. Clim. Past 16, 2547–2571. https://doi.org/10.5194/cp-16-2547-2020. URL.
Sarnthein, M., Grootes, P.M., Mudelsee, M., 2023. Centennial to millennial-sale fluctuations of the Lake Suigetsu atmospheric ^{14}C record represent real ^{14}C features over last glacial-to-deglacial times. Radiocarbon 65 (4). https://doi.org/10.1017/RDC.2023.47.
Schlitzer, R., 2002. Interactive analysis and visualization of geoscience data with Ocean Data View. Comput. Geosci. 28, 1211–1218.
Sessford, E.G., Tisserand, A.A., Risebrobakken, B., Andersson, C., Dokken, T., Jansen, E., 2018. High-resolution benthic Mg/Ca temperature record of the intermediate water in the Denmark Strait across D-O stadial-interstadial cycles. Paleoceanogr. Paleoclimatol. 33, 1169–1185. https://doi.org/10.1029/2018PA003370.
Sessford, E.G., Jensen, M.F., Tisserand, A.A., Muschitiello, F., Dokken, T., Nisancioglu, K. H., Jansen, E., 2019. Consistent fluctuations on intermediate water temperature off the coast off Greenland and Norway during Dansgaard-Oeschger events. Quat. Sci. Rev. 223, 1–17, 105887.
Siedler, G., Church, J., Gould, J. (Eds.), 2001. Ocean Circulation and Climate. Observing and Modelling the Global Ocean. Academic Press, San Diego - New York, pp. 1–715.
Simstich, J., Sarnthein, M., Erlenkeuser, H., 2003. Paired δ^{18}O signals of *Neogloboquadrina pachyderma* (s) and *Turborotalita quinqueloba* show thermal stratification structure in Nordic Seas. Mar. Micropaleontol. 48, 107–125.
Simon, M.H., Rutledal, S., Menviel, L., Zolles, T., Haflidason, H., Born, A., Berben, S.M., Dokken, T.M., 2023. Atlantic inflow and low sea-ice cover in the nordic seas promotes fennoscandian ice sheet growth during the last glacial maximum. Communications Earth and Environment 4, 385. https://doi.org/10.1038/s43247-0223-01032-9.
Struve, T., Roberts, N.L., Frank, M., Piotrowski, A.M., Spielhagen, R.F., Gutjahr, M., Teschner, C., Bauch, H.A., 2019. Ice-sheet-driven weathering input and water mass mixing in the Nordic Seas during the last 25,000 years. Earth Planet Sci. Lett. 514, 108–118.
Svensson, A., Andersen, K.K., Bigler, M., Clausen, H.B., Dahl-Jensen, D., Davies, S.M., Johnsen, S.J., Muscheler, R., Parrenin, F., Rasmussen, S.O., Röthlisberger, R., Seierstad, I., Steffensen, J.P., Vinther, B.M., 2008. A 60,000-year Greenland stratigraphic ice core chronology. Clim. Past 4, 47–57.
Thornalley, D.J.R., Barker, S., Broecker, W.S., Elderfield, H., McCave, I.N., 2011. The deglacial evolution of the North Atlantic deep convection. Science 331, 202–205.
Trauth, M.H., Sarnthein, M., Arnold, M., 1997. Bioturbational mixing depth and carbon flux at the sea floor. Paleoceanography 12, 517–526.
Våge, K., Pickart, R.S., Spall, M.A., et al., 2011. Significant role of the North Iceland Jet in the formation of Denmark Strait overflow water. Nat. Geosci. 4. https://doi.org/10.1038/NGEO1234.
Van Kreveld, S., Sarnthein, M., Erlenkeuser, H., Grootes, P., Jung, S., Nadeau, M.J., Pflaumann, U., Voelker, A., 2000. Potential links between surging ice sheets, circulation changes, and the Dansgaard-Oeschger cycles in the Irminger Sea. Paleoceanography 15, 425–442.
Voelker, A., 1999. Dansgaard-Oeschger Events in Ultra-high Resolution Sediment Records from the Nordic Seas, vol. 9. Berichte-Reports Institut für Geowissenschaften, University of Kiel, pp. 1–278.
Voelker, A.H.L., Grootes, P.M., Nadeau, M.J., Sarnthein, M., 2000. ^{14}C levels in the Iceland Sea from 25-53 kyr and their link to the Earth's magnetic field intensity. Radiocarbon 42 (3), 437–452.
Voelker, A.H.L., Haflidason, H., 2015. Refining the Icelandic tephrachronology of the last glacial period – the deep-sea core PS2644 record from the southern Greenland Sea. Global Planet. Change 131, 32–62.
Voelker, A., Sarnthein, M., Grootes, P.M., Erlenkeuser, H., Laj, C., Mazaud, A., Nadeau, M., Schleicher, M., 1998. Correlation of marine ^{14}C ages from the Nordic Seas with the GISP2 Isotope record: implications for radiocarbon calibration beyond 25 kyr. Radiocarbon 40, 517–534.
Waelbroeck, C., Skinner, L.C., Labeyrie, L., Duplessy, J.-C., Michel, E., Riveiros, N.V., Gherardi, J.-M., Dewilde, F., 2011. The timing of deglacial circulation changes in the Atlantic. Paleoceanography 26, PA3213. https://doi.org/10.1029/2010PA002007.
Weinelt, M., Sarnthein, M., Vogelsang, E., Erlenkeuser, H., 1991. Early decay of the Barents Shelf ice shelf – spread of stable isotope signals across the eastern Norwegian Sea. Norsk Geologisk Tidsskift 71, 137–140.
Weinelt, M., Vogelsang, E., Kucera, M., Pflaumann, U., Sarnthein, M., Voelker, A., Erlenkeuser, H., Malmgren, B.A., 2003. Variability of North Atlantic heat transfer during MIS 2. Paleoceanography 18, 1–16. https://doi.org/10.1029/2002PA000772.
Whitehead, J.A., Leetmaa, A., Knox, R.A., 1974. Rotating hydraulics of strait and sill flows. Geophys. Fluid Dynam. 6, 101–125.
Wolff, E.W., Chappelaz, J., Blunier, T., Rasmussen, S.O., Svensson, A., 2010. Millennial-scale variability during the last glacial: the ice core record. Quat. Sci. Rev. 29, 2828–2838. https://doi.org/10.1016/j.quascirev.2009.10.013.
You, D., Stein, R., Fahl, K., Williams, M.C., Schmidt, D.N., McCave, I.N., Barker, S., Schefuß, Niu, L., Kuhn, G., Niessen, F., 2023. Last deglacial abrupt climate changes caused by meltwater pulses in the Labrador Sea. Communications Earth & Environment 4, 81. https://doi.org/10.1038/s43247-023-00743-3.